

AD-757 484

INFRARED STUDIES OF GASEOUS DISCHARGES

John Strong

Massachusetts University

Prepared for:

Air Force Cambridge Research Laboratories  
Advanced Research Projects Agency

30 November 1972

DISTRIBUTED BY:

**NTIS**

National Technical Information Service  
U. S. DEPARTMENT OF COMMERCE  
5285 Port Royal Road, Springfield Va. 22151

AD757484

INFRARED STUDIES OF GASEOUS DISCHARGES

by  
John Strong

Astronomy Research Facility  
Department of Physics and Astronomy  
University of Massachusetts  
Amherst, Massachusetts 01002

Contract No. F19628-72-C-0075  
Project No. 5130

FINAL REPORT

Period Covered: 1 November 1971 to 30 November 1972

30 November 1972

Contract Monitor: Donald R. Smith  
Optical Physics Laboratory

Approved for public release; distribution unlimited

Sponsored by

Advanced Research Projects Agency  
ARPA Order No. 1366

Prepared for

Air Force Cambridge Research Laboratories  
Air Force Systems Command  
United States Air Force  
Bedford, Massachusetts 01730

Reproduced by  
NATIONAL TECHNICAL  
INFORMATION SERVICE  
U S Department of Commerce  
Springfield VA 22131



ARPA Order No. 1366

Program Code No. 1E50

Contractor: University of Massachusetts


Effective Date of Contract: 7 October 1971

Contract No. F19628-72-C-0075

Principal Investigator and Phone No.  
Prof. John Strong/413 545-0163

AFCRL Project Scientist and Phone No.  
Donald R. Smith/617 861-2504

~~Contract Expiration~~ Date: 30 November 1972

ACCESSION FOR	
NTIS	White Section <input checked="" type="checkbox"/>
DDC	Bull Section <input type="checkbox"/>
UNANNOUNCED	
JUSTIFICATION	
BY	
DISTRIBUTION/AVAILABILITY CODES	
DISC.	AVAIL. AND/OR SPECIAL
	

Qualified requestors may obtain additional copies from the Defense Documentation Center. All others should apply to the National Technical Information Service.

INFRARED STUDIES OF GASEOUS DISCHARGES  
by  
John Strong

Astronomy Research Facility  
Department of Physics and Astronomy  
University of Massachusetts  
Amherst, Massachusetts 01002

Contract No. F19628-72-C-0075  
Project No. 5130

FINAL REPORT

Period Covered: 1 November 1971 to 30 November 1972

30 November 1972

Contract Monitor: Donald R. Smith  
Optical Physics Laboratory

Approved for public release; distribution unlimited.

Sponsored by

Advanced Research Projects Agency  
ARPA Order No. 1366

Prepared for

Air Force Cambridge Research Laboratories  
Air Force Systems Command  
United States Air Force  
Bedford, Massachusetts 01730

UNCLASSIFIED

Security Classification

## DOCUMENT CONTROL DATA - R &amp; D

(Security classification of title, body of abstract and indexing annotation must be entered when the overall report is classified)

1. ORIGINATING ACTIVITY (Corporate author) University of Massachusetts Astronomy Research Facility Amherst, Massachusetts 01002		2a. REPORT SECURITY CLASSIFICATION UNCLASSIFIED	
		2b. GROUP	
3. REPORT TITLE  INFRARED STUDIES OF GASEOUS DISCHARGES			
4. DESCRIPTIVE NOTES (Type of report and inclusive dates) Scientific. Final. 1 November 1971-30 November 1972		Approved: 3 Jan 1973	
5. AUTHOR(S) (First name, middle initial, last name)  John Strong			
6. REPORT DATE 30 November 1972	7a. TOTAL NO OF PAGES 126	7b. NO OF REFS 4	
8a. CONTRACT OR GRANT NO F19628-72-C-0075 ARPA Order 1366		9a. ORIGINATOR'S REPORT NUMBER(S) UMASS-ARF-72-274	
b. PROJECT NO Task, Work Unit Nos. 5130 n/a n/a			
c. Dod Element 62301D		9b. OTHER REPORT NO(S) (Any other numbers that may be assigned this report) AFCRL-72-0739	
d. Dod Subelement n/a			
10. DISTRIBUTION STATEMENT  A - Approved for public release; distribution unlimited.			
11. SUPPLEMENTARY NOTES  TECH, OTHER		12. SPONSORING MILITARY ACTIVITY Air Force Cambridge Research Laboratories (OP) L.G. Hanscom Field Bedford, Massachusetts 01730	
13. ABSTRACT  Preparations for study of the chemistry of discharges have been made. Pure water vapor absorption measurements in the 6.3 $\mu$ band have been conducted using the Hadamard Transform Spectrometer with resolving power of .07 cm <sup>-1</sup> .  An investigation of the infrared spectrum of H discharge is described.  The emission spectrum of superheated steam (600°C) has been studied with the observation of many new hot lines.			

DD FORM 1 NOV 65 1473

-2-

UNCLASSIFIED

Security Classification

UNCLASSIFIED

Security Classification

14	KEY WORDS	LINK A		LINK B		LINK C	
		ROLE	WT	ROLE	WT	ROLE	WT
	Infrared Emission Studies Hadamard Transform Spectrometer Infrared Spectrum of H Discharge Emission Spectrum of Superheated Steam						

UNCLASSIFIED

Security Classification

### TECHNICAL REPORT SUMMARY

We developed and fabricated a Hadamard Transform Spectrometer under a previous support budget (ARPA Contract F19628-70-C-0296). Under the present contract (ARPA Contract F19628-72-C-0075), we have adapted the spectrometer to double pass--with chopping between the two passes (to suppress scattered light). This latter arrangement gives a resolving power  $\Delta\nu = .07 \text{ cm}^{-1}$ . The slits are the same as the Hadamard Transform Spectrometer slits, and cannot be made smaller. The spectrum that exhibited this resolution is reproduced in Fig. 2 of the paper, "Pure Water Vapor Absorption Measurements in 6.3 Micron Band" (Attachment A).

We have separately provided the Hadamard Transform Spectrometer with KI-KBr achromatic lenses for  $\lambda\lambda$  8 to  $22\mu$  in addition to KBr-NaCl achromats for  $\lambda\lambda$  5 to  $12\mu$ .

Under ONR support, but using the above-mentioned Hadamard Transform Spectrometer, we provided a special all-glass, atomic hydrogen discharge tube to simulate the experiments of Humphreys that led to the discovery of the first line of the atomic series beyond the Pfund series, at  $12.37\mu$ . We made this precursor study of the hydrogen discharge, along with other experiments, as an introduction to discharges in the large absorption cell--to determine the manner in which infrared emission lines appear. An attached paper, "The Seventh Series of Atomic Hydrogen," (Attachment B) reports observation of the  $12.37\mu$  line, and the  $8\rightarrow 7$  first line of the seventh H series, at  $19.06\mu$ .

We have interfaced the Hadamard Transform Spectrometer to our 100 ft. absorption cell (with 300 ft. optical path) for study of other discharges. AC discharges have been studied in this cell. The discharge is between a 3 in. diameter, central aluminum electrode of 37 ft. length (co-axial with the absorption cell) and the cell wall which is 3 ft. in diameter. But owing to delays of procurement, we have not yet been able to get gas analysis of the large discharge. The gas composition is different from that admitted owing to outgassing of the steel cell wall surfaces. Now a mass spectrometer is being delivered which will allow the analysis of the discharge gas.  $H_2O$  concentrations are of particular importance.

The power supply up to now has been a transformer of less than 1 ampere capacity. Now we have 10 amperes capacity (two 10 KVA transformers of 2000v. max. output, which we can operate over-capacity for short periods).

The absorption cell is routinely pumped by our pumping system to less than  $1\mu$  pressure and the discharges are operated at pressures ranging from this limit to  $1/10$  to  $2/10$  mm Hg pressure.

After the mass spectrometer will be installed, we plan to study discharges in the "astronomical gases"  $O_2$ ,  $N_2$ ,  $CO_2$ ,  $H_2O$  and  $NH_3$  separately, and in various combinations. Concurrently with taking of infrared spectra we plan to measure the DC discharge current; gas pressure; the chemical composition of the discharge (with our mass spectrometer); and the electron and ion kinetic temperatures with Langmuir probes.

We undertook the study of the hydrogen discharge with our Hadamard Transform Spectrometer, in part, because another study of infrared absorption spectra was slow in getting finished with the absorption cell.

Some effort has been expended in finishing the absorption and emission spectra of superheated steam ( $600^\circ C$ ). We have used a Perkin-Elmer 210-B grating

spectrometer worked at a resolving power:  $\lambda / \Delta \lambda \sim 0.5 \text{ cm}^{-1}$ . This study was begun under Contract F19628-70-C-0296, and all the spectra have now been determined. These spectra revealed many new hot lines that will be encountered in subsequent studies of discharge spectra of  $\text{H}_2\text{O}$ --possibly in greater strength than the presently known lines that originate from levels of room temperature excitation. This work will be published as partly sponsored by the subject Contract F19628-72-C-0075 after the spectra are fully analyzed. The spectra are being supplied to Dr. McClatchey who has agreed to supply us with calculated synthetic spectra. These synthetic spectra will be calculated using the same conditions of path length, steam temperature and scanning function under which they were observed. An attachment (Attachment C) reports these spectra.

In addition to this forthcoming report on superheated steam, we have given two papers supported by the subject Contract (Attachments A and D). They relate to the equipment that was developed under the predecessor contract and adapted to the glow discharge experiments, as set forth above.

## PERSONNEL

Principal Investigator: Dr. John Strong  
Research Engineer: Peter Hansen  
Electronics Engineer: Ta-Chun Li  
Graduate Students: Harold Heaton )  
Shau-Yau Ho ) Research  
Support Staff: William Dalton-Administrative  
Linda Barron-Secretarial,  
Reports, etc.  
Ernest Provo-Machine Shop,  
Assembly, etc.

FACILITIES ACQUIRED

This Contract provided for the purchase of a mass spectrometer, jointly financed by ARPA Contract 19628-72-C-0075, and ONR Contract #N00014-67-A-030-0001, but not installed as of this date.

ACKNOWLEDGMENT

This research was supported by the Advanced Research Projects Agency of the Department of Defense, and was monitored by Air Force Cambridge Research Laboratories under Contract No. F19628-72-C-0075.

REFERENCES (Attached).

- A. P. Hansen and J. Strong, "Pure Water Vapor Absorption Measurements in 6.3 Micron Band," presented at OSU Symposium on Molecular Structure and Spectroscopy, Columbus, Ohio (June, 1972).
- B. P. Hansen and J. Strong, "The Seventh Series of Atomic Hydrogen," Appl. Opt. (in press--February, 1973 issue).
- C. Shau-Yau Ho, "Infrared Absorptions and Emissions of Superheated Steam," Astronomy Research Facility Report #275 (November, 1972).
- D. P. Hansen and J. Strong, "High Resolution Infrared Spectrometer with Multiplex Advantage," presented at Electro-Optics Systems Design Conference, New York City, (September, 1972), published in EOSD '72 proceedings.

PURE WATER VAPOR ABSORPTION MEASUREMENTS  
IN 6.3 MICRON BAND

Peter Hansen  
John Strong

Astronomy Research Facility  
Department of Physics and Astronomy  
University of Massachusetts  
Amherst, Massachusetts 01002

June 1972

ABSTRACT

Water vapor absorption lines from 1400 to 1700  $\text{cm}^{-1}$  are studied at 0.07  $\text{cm}^{-1}$  resolving power using our Hadamard Transform Spectrometer.<sup>1</sup> This includes the lines reported by Fridovich and Kinard<sup>2</sup> last year. The absorption path conditions are the same: 92-meter geometrical path through pure water vapor at  $p < 10$  mm Hg.

The purpose of this investigation is to check  $S_v$  values in the literature against observations as they apply to conditions near those that obtain in the interstellar medium.

Hansen & Strong / 2

Experimentally verified values of line strength (S) and half width ( $\gamma$ ) for water vapor and carbon dioxide absorption lines are of importance in the determination of temperature and pressure profiles in the atmosphere from spectra observed by space vehicles.

Equivalent widths of three water vapor lines have been preliminarily measured. They were observed over a long path with water vapor at low pressure to insure negligible overlapping. This is the beginning of a program to check currently established S· $\gamma$  values for many lines in CO<sub>2</sub> and H<sub>2</sub>O absorption bands from 2000 to 400 cm<sup>-1</sup>.

The path length of the absorption cell (Fig. 1) is 92 meters. The pressures are less than 10 mm pure water vapor. The instrumentation gives 0.07 cm<sup>-1</sup> resolution, as indicated in Fig. 2.

Table I presents the calculated and observed equivalent widths for the three lines indicated in the water vapor spectra of Fig. 3. Although these results are preliminary in certain respects, as set forth below, the consistent discrepancy of 23% seems significant--but unaccountable at the present time.

Hansen & Strong / 3

The order sorting filter that was used in the helium cooled detector of the spectrometer, for these spectra, was inadequate to give us a free spectral range. We measured both the eighth and ninth orders overlapped. But the three lines were all substantially opaque over the span of the scanning function so that their central dip represents  $A_0 = 100\%$ . In our program, later, we will use an LN-2 cooled pre-disperser. With it this free spectral range problem will disappear as we will obtain less than one free spectral range over the grating scan. This pre-disperser was not available for this report. We used a self broadening factor of  $5.49^3$  to calculate  $\gamma$ :  
 $5.49 P \gamma^0 = \gamma$ .

We have developed a reduction procedure which was described here last year.<sup>4</sup> The lines we measure, if Lorentzian, all have the same contour if absorption is plotted as function of  $x$  as abscissa:

$$A = 1 - e^{-\pi/x^2}$$

$$x = \frac{\nu - \nu_0}{\gamma Z} \quad \text{where } Z = \frac{\sqrt{S u}}{\sqrt{\pi^2 \gamma}} = \frac{1}{2\pi} W .$$

This formulation is adequate if  $Z > \pi$ . For example, the values used for the three lines analyzed were in the range  $\pi^3 < Z < \pi^4$ .

Furthermore, Heaton<sup>5</sup> has developed equations to calculate  $W_{12}$  for overlapping lines for cases where the two lines are nearly coincident, and  $W_{12}$  varies from  $\sqrt{W_1^2 + W_2^2}$  by up to 10%; and where the two lines are nearly independent, and  $W_{12}$  varies from  $(W_1 + W_2)$  by up to 10%.

The effect of Doppler widening takes a simple form for a line observed under our extreme conditions of long path and low pressure. Then,

$$T = e^{-\frac{\pi V(x,z)}{x^2}} \quad \text{where}$$

$$V = \sqrt{\frac{m}{2\pi kT}} \int_{-\infty}^{\infty} \frac{e^{-\left(\frac{mv}{2\pi kT}\right)^2}}{\left[1 - \left(\frac{v_0}{v-v_0}\right)\frac{v}{c}\right]^2 + \left(\frac{v}{v-v_0}\right)^2} dv.$$

The effect of the coefficient  $V$  is negligible: Table II gives values of  $W$  calculated, with  $V(x,z)$ , for the conditions under which we observed.

Table II

$Z$ <u><math>P_{\text{torr}}</math></u>	<u><math>\pi</math></u>	<u><math>\pi^2</math></u>	<u><math>\pi^3</math></u>	<u><math>\pi^4</math></u>	<u><math>\pi^5</math></u>
0.5-	.55	.10	.03	0	0
1.0	.15	.03	0	0	0
2.0	.10	0	0	0	0
4.0	.02	0	0	0	0
8.0	0	0	0	0	0

The HTS spectrometer<sup>1</sup> described here last year gives diffraction limited resolving power when used as a conventional double pass spectrometer. This spectrometer as used for this study is shown in Fig. 4. The multiplex advantage of HTS, not needed with our helium cooled detector, would be useful if a less sensitive detector were used. Since our bolometer had good sensitivity ( $10^{-13} \text{ WHz}^{-1/2}$ ), single slit scanning was sufficient.

An echelle affords the best dispersing means for infrared spectroscopy, once the free spectral range problem is solved. This is because infrared spectroscopy is usually energy limited even with a helium cooled

bolometer. If energy limited, the energy available is proportional to spectral dispersion, which in turn is proportional to the tangent of the grating angle.

This, with an ordinary grating with a  $20^\circ$  blaze is  $\tan 20^\circ = 0.364$  while, for the echelle,  $\tan 63^\circ 26' = 2.000$ . Thus the echelle gives a gain by the factor 5.24. The echelle facets yield a high blaze efficiency, throughout one free spectral range, of  $> 50$  to 100%.

Achromatic doublet lenses have been used and they yield diffraction limited resolution over their useful wavelength ranges:  $\lambda\lambda$  5 to  $13\mu$  for the NaCl-KBr lens; and  $\lambda\lambda$  7 to  $24\mu$  for the KBr-KI lens.

#### Acknowledgment

This research was supported by the Advanced Research Projects Agency (ARPA) under Contract No. F19628-72-C-0075.

TABLE I

<u><math>\nu</math></u>	<u>P</u>	<u><math>W_c</math></u>	<u><math>W_o</math></u>	<u><math>W_c / W_o</math></u>
1662.8	1 mm	.295	.392	.752
	2 mm	.591	.775	.762 .757
1646.0	1 mm	.395	.479	.824
	2 mm	.789	1.070	.737 .781
1623.6	1 mm	.304	.404	.752
	2 mm	.607	.749	.789 .771 .770

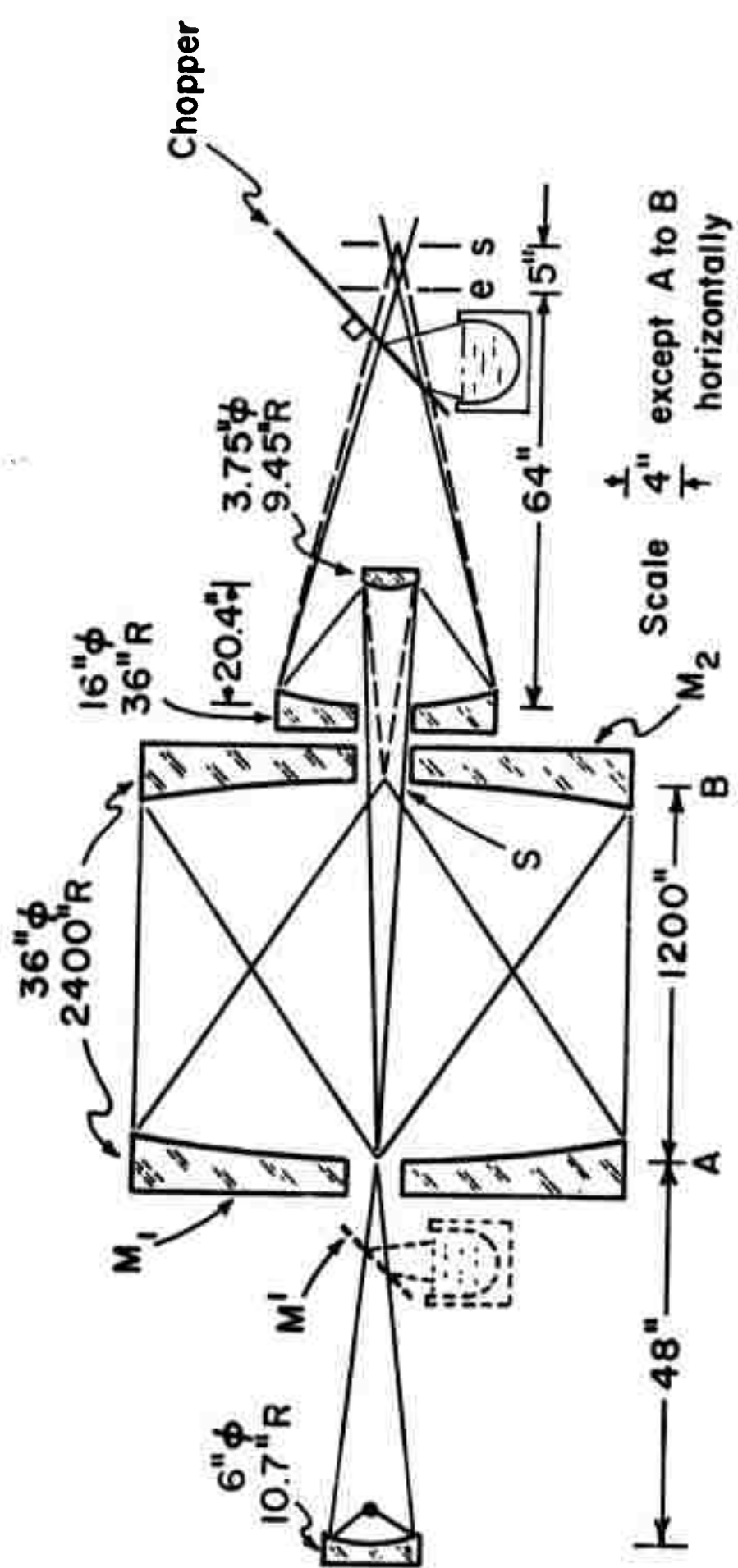


Fig. 1



Fig. 2. High Resolution Spectra. (a) Water Vapor At  $P = 0.300$  mm, 92 m Path Length. (b) Carbon Dioxide At  $P = 20$  mm, 2.2 m Path Length.

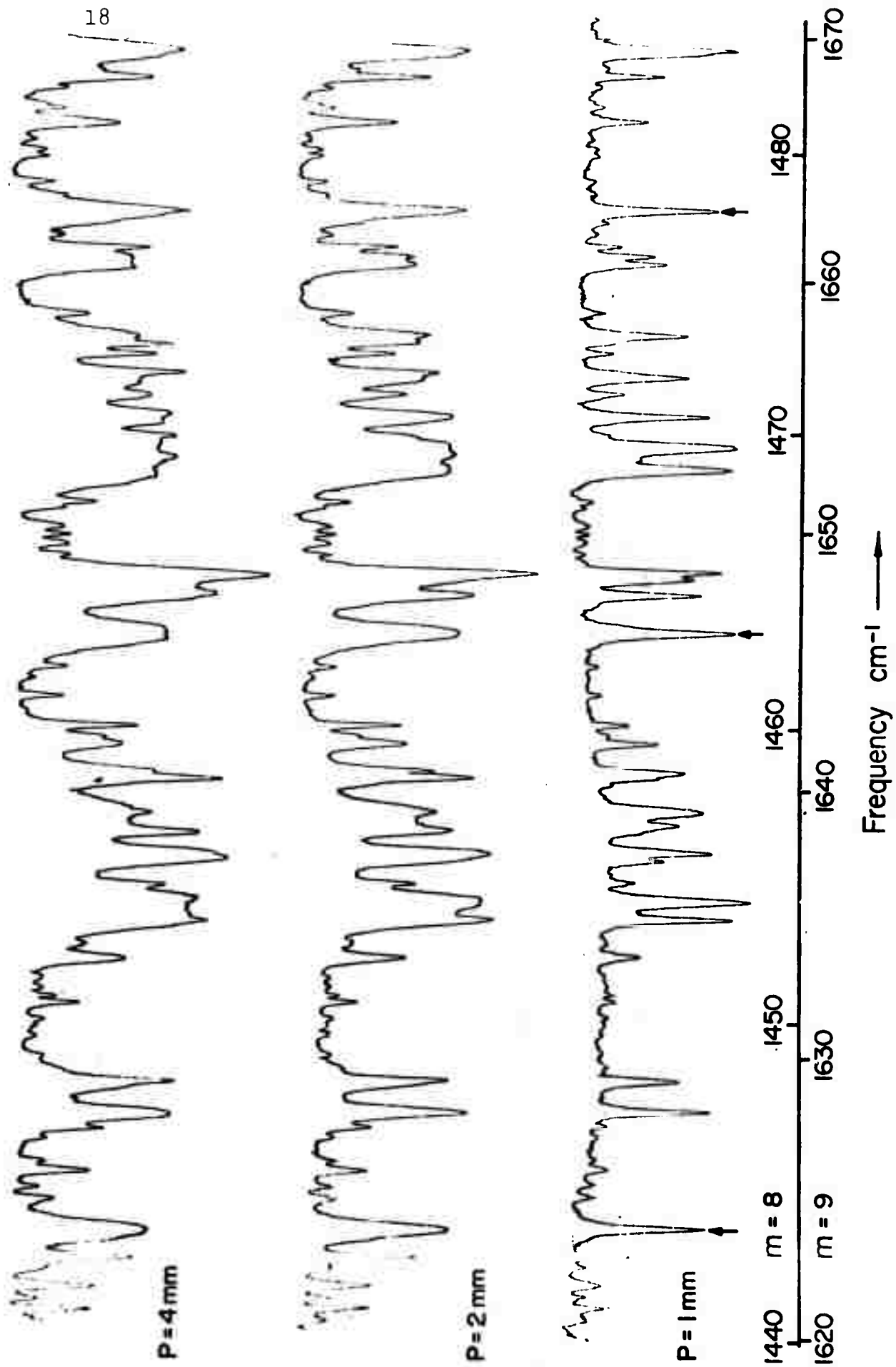


Fig. 3. Water Vapor Absorption At Three Pressures Over 92 Meter

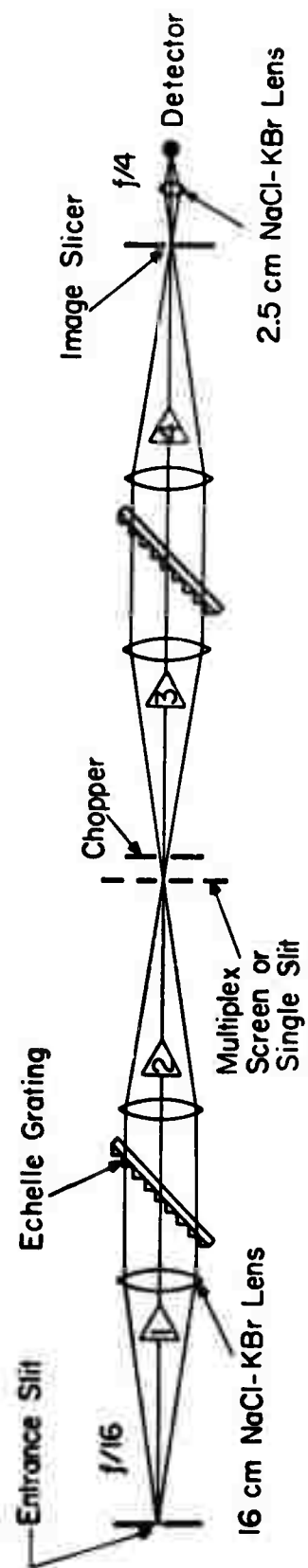
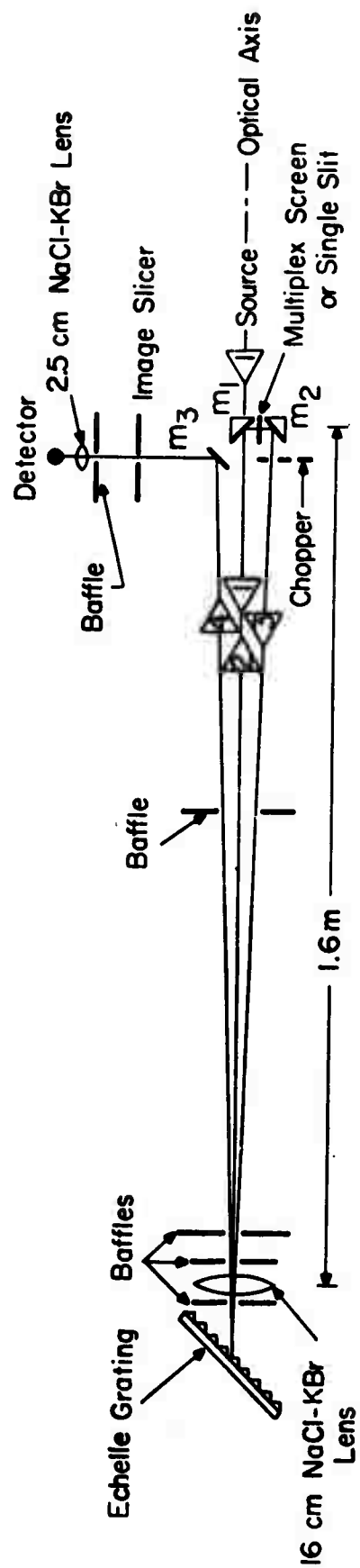


Fig. 4

Hansen & Strong / 12

References:

1. P. Hansen and J. Strong, Appl. Opt. 11, 502 (1972).
2. B. Fridovich and J. R. Kinard, J. Opt. Soc. Am. 62, 542 (1972).
3. W. S. Benedict and R. F. Calfee, "Line Parameters for the 1.9 and 6.3 Micron Water Vapor Bands," ESSA Professional Paper 2, U.S. Department of Commerce, June 1967. This is available from the Superintendent of Documents, U.S. Government Printing Office, Washington, D.C. 20402.
4. J. Strong, "On Interpretation of Infrared Absorption Lines," Appl. Opt., in press (November 1972).
5. H. I. Heaton, "Selecting Infrared Absorption Lines With Innocuous Neighbors," Appl. Opt., in press (November 1972).

## ATTACHMENT B

## THE SEVENTH SERIES OF ATOMIC HYDROGEN

Peter Hansen  
John Strong

Astronomy Research Facility  
Department of Physics and Astronomy  
University of Massachusetts  
Amherst, Massachusetts 01002

November, 1972

The list of first lines of various atomic hydrogen series, after Prof. Pfund's paper,<sup>1</sup> is extended in Table I to include the new line discovered by Humphreys<sup>2</sup> and a new line of the next series. In this paper we show the spectra of the last two lines. The first experimental realizations of the lines  $5 \rightarrow 4$ ,  $6 \rightarrow 4$ ; and  $6 \rightarrow 5$  were predicated by Pfund's development of a very sensitive thermocouple detector.<sup>3</sup> The spectra here of  $7 \rightarrow 6$  and  $8 \rightarrow 7$  were similarly predicated by a further bolometer development, combined with an efficient echelle grating used with infrared achromatic lens optics.<sup>4</sup> In addition, a discharge tube, similar to that used by Humphreys, was provided with adequate controls to enable optimizing the H spectrum.

TABLE I

<u>Series</u>	<u><math>\Delta m</math></u>	<u><math>\lambda</math> in <math>\mu</math></u>
Lyman	2 $\rightarrow$ 1	.1216
Balmer	3 $\rightarrow$ 2	.6565
Paschen	4 $\rightarrow$ 3	1.8756
Brackett	5 $\rightarrow$ 4	4.0523
Pfund	6 $\rightarrow$ 5	7.4599
Humphreys	7 $\rightarrow$ 6	12.372
New	8 $\rightarrow$ 7	19.062

The wavelength (the first member of the seventh series of atomic hydrogen) agrees with the theoretical value of  $19.062\mu$  ( $524.60\text{ cm}^{-1}$ ), the exact determination being limited by the spectral resolving power of the instrumentation. Previously, the first member of the sixth series has been successfully measured by Humphreys, who also suggested the use of pure water vapor as a source for the hydrogen atoms.

The experimental apparatus consisted of a water-cooled discharge tube used end on and placed immediately in front of the spectrometer entrance slit. Fig. 1 illustrates the discharge tube which is surrounded by a water jacket through which a continuous flow of tap water provides the necessary cooling. A small flask containing distilled water serves as the source of hydrogen atoms. To obtain the most intense atomic hydrogen spectrum, we were able to finely control the amount of water vapor admitted to the tube and the pressure

in the tube (i.e. the flow rate) by means of two high precision capillary valves. The spectrum of the discharge tube was continuously monitored in the visible, where the disappearance of the molecular bands and the intensification of the first four Balmer lines indicated a good atomic hydrogen discharge.<sup>5</sup> In addition, the discharge current was kept at a high value to optimize the H spectrum.

The power supply consisted of a PTC 5KVA powerline transformer operated in reverse by a 30 AMP variac. In addition, to allow for some independent control of voltage and current, a bank of oil-cooled power resistors was placed in series with the discharge tube. The electrodes were slotted aluminum cylinders that fitted tightly against the glass walls for maximum cooling. The tube was operated near 1000 VAC and the best atomic hydrogen spectra obtained were in the current range of .250 to .400 amperes, resulting in a current density in the discharge column of 1.25 to 2 amperes/cm<sup>2</sup>.

The spectrometer<sup>6</sup> uses alkaline halide achromats, an echelle grating and a bolometer cooled to liquid helium temperatures. It is continuously purged with dry air to eliminate all detectable traces of water vapor and carbon dioxide. Under good signal to noise conditions, a resolving power of .07 cm<sup>-1</sup> is achieved. A He-Ne laser was used to align the discharge tube with the optic axis of the spectrometer to assure a maximum signal.

Fig. 2 shows the first member of the Humphreys series  $12.37\mu$  ( $808.28 \text{ cm}^{-1}$ ). The entrance and exit slits were widened to .6 mm with a resulting estimated resolving power of .7 to  $.3 \text{ cm}^{-1}$ . Wavelength calibration was accomplished with the well known carbon dioxide spectrum as a reference. We did not attempt to measure the second member of this series ( $7.502\mu$ ) for lack of a proper cold filter at the detector.

Fig. 3 represents the first member  $19.062\mu$  ( $524.60 \text{ cm}^{-1}$ ) of the seventh series. The discharge tube was operated at the optimum conditions determined from the much stronger Humphreys line, typical values being ( $I \sim .350 \text{ A}$ ,  $V \sim 1000 \text{ VAC}$ ,  $P \sim .8 \text{ mm Hg}$ ). In addition, since an extremely low signal level was involved, the large rotating chopper in the spectrometer was replaced with a tuning fork chopper to eliminate the last small amount of microphonic noise in the detector. Also, the slits were widened (1 mm entrance, 1.3 mm exit). The  $19\mu$  water vapor bands<sup>7</sup> were used as a reference for wavelength calibration here. A water vapor spectrum (Fig. 3a) taken with the same resolution as the  $19.06\mu$  line is also shown. This was obtained by admitting room air to the spectrometer. A Nernst glower was the source. The equivalent absorption path was 8 meters at a pressure of 1 ATM.

#### Acknowledgments

This work was supported under ONR Contract #N00014-67-A-0230-0002.

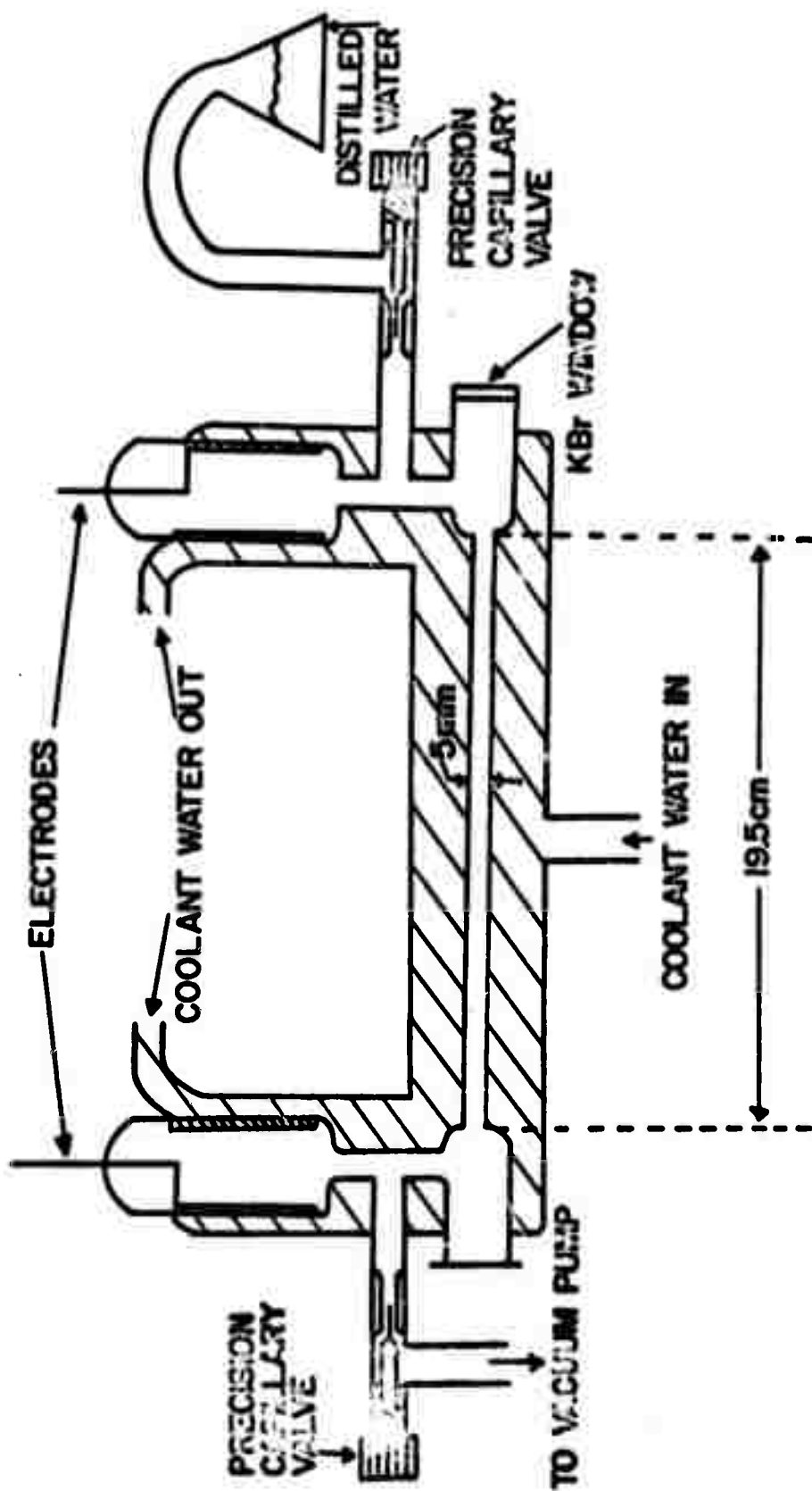


FIG. 1 SCHEMATIC REPRESENTATION OF THE DISCHARGE TUBE

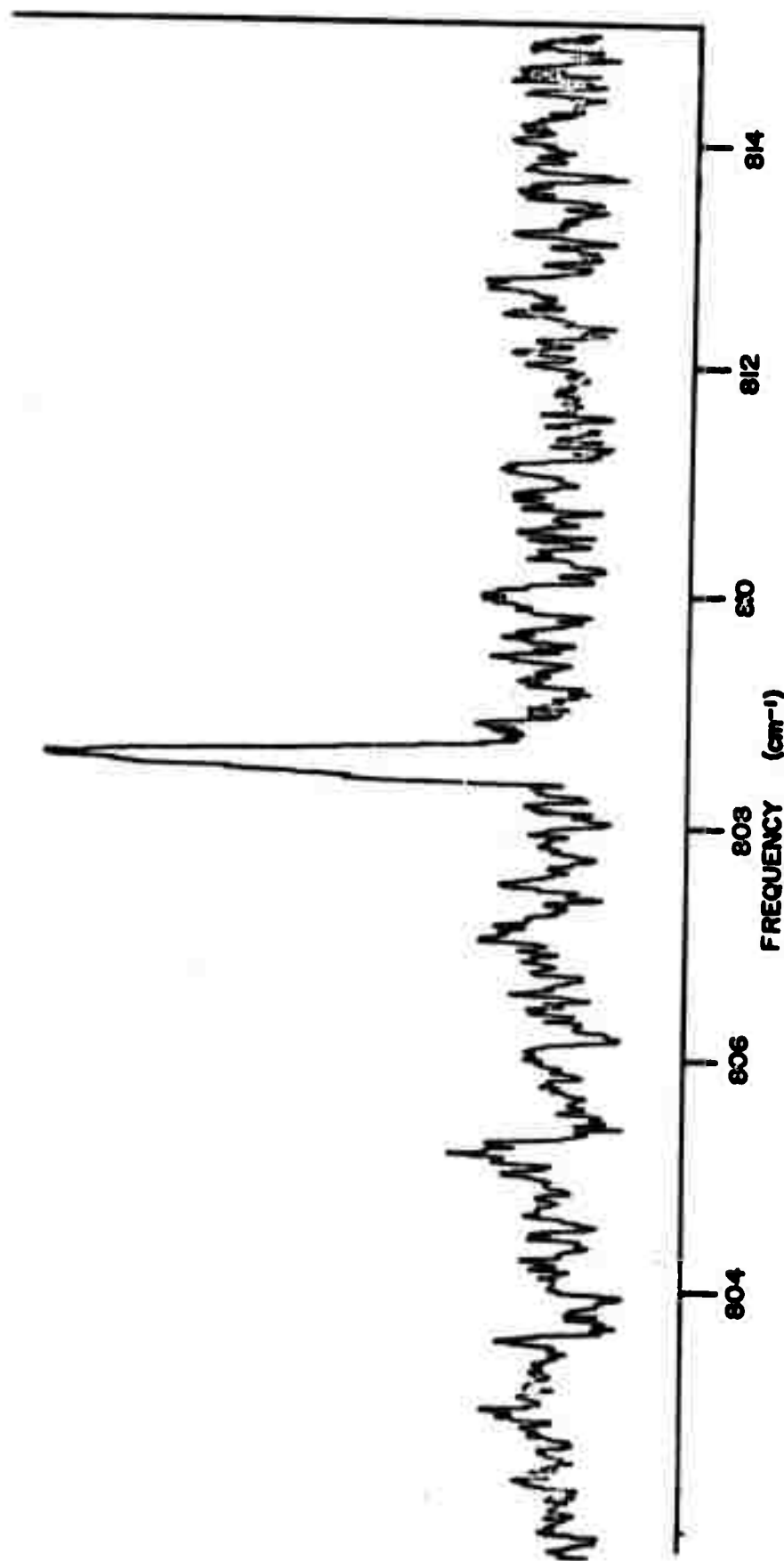


FIG. 2 THE FIRST MEMBER OF THE HUMPHREYS SERIES ( $n_1 = 6$ ). BOTH ENTRANCE AND EXIT SLITS WERE OPENED TO 0.7 mm.

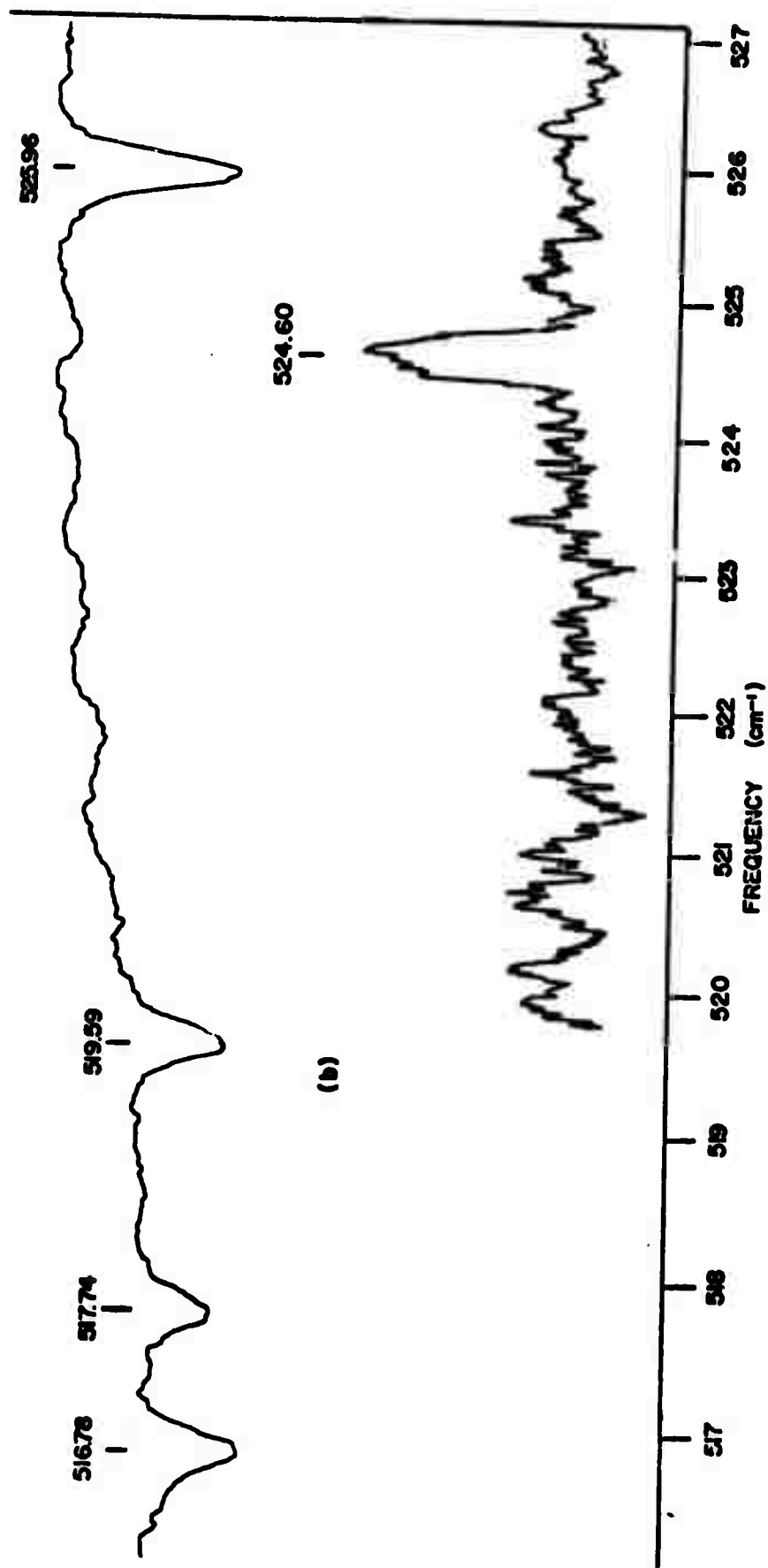


FIG. 3 THE FIRST MEMBER OF THE SEVENTH SERIES. (b) ALONG WITH A WATER VAPOR SPECTRUM. (a) IN THE SAME SPECTRAL REGION. THE SPECTROMETER SLITS WERE SET AT THEIR MAXIMUM WIDTH.

REFERENCES

1. A. H. Pfund, "The Emission of Nitrogen and Hydrogen in the Infrared," J. Opt. Soc. Am. 2, No. 3 (Sept., 1924).
2. Curtis J. Humphreys, "The Sixth Series in the Spectrum of Atomic Hydrogen," Journal of Research of the National Bureau of Standards 50, No. 1 (January, 1953).
3. F.S. Brackett, "Visible and Infra-Red Radiation of Hydrogen," Astrophys. J. 56, 159 (1923).
4. John Strong, "Achromatic Doublet Lenses for Infrared Radiation," Appl. Opt. 10, 1439 (1971); 11, 2331 (1972).
5. R.W. Wood, "An Extension of the Balmer Series of Hydrogen and Spectroscopic Phenomena of very Long Vacuum Tubes," Proc. of Royal Soc. A. 91, (1920).
6. Peter Hansen and John Strong, "High Resolution Hadamard Transform Spectrometer," Appl. Opt. 11, No. 3, (March, 1972).
7. K. Narahari Rao, L.R. Ryan, H.H. Nielsen, J. Opt. Soc. Am. 49, 216 (1959).

INFRARED ABSORPTIONS AND EMISSIONS  
OF SUPERHEATED STEAM

by Shau-Yau Ho

Astronomy Research Facility  
Department of Physics and Astronomy  
University of Massachusetts  
Amherst, Massachusetts 01002

November, 1972

ABSTRACT

Both absorption spectra and emission spectra of superheated steam at 600°C have been obtained under high resolution from 3000  $\text{cm}^{-1}$  to 2000  $\text{cm}^{-1}$  and from 1260  $\text{cm}^{-1}$  to 615  $\text{cm}^{-1}$ . These higher energy level spectra are not observable at room temperature. Approximately 400 lines have been observed between 3.29 $\mu$  and 5.06 $\mu$  in the short wavelength range, and 700 lines between 7.91 $\mu$  and 16.25 $\mu$  in the long wavelength range. There is an absorption-free region at 600°C lying between 2750  $\text{cm}^{-1}$  and 2485  $\text{cm}^{-1}$ . Spectra of all bands are shown and spectral positions are measured and tabulated. Results are compared with other experiments and theoretical computations.

## INTRODUCTION

It has long been this laboratory's interest to investigate all the water vapor spectra from  $2\mu$  to  $40\mu$ . These measurements are important for both practical and theoretical reasons. The results find practical application in a number of fields including military problems, remote sensing from spacecraft, air pollution detections, etc., related to the transmission of infrared radiation through the atmosphere, and its emission. They are also important in the study of the heat balance of the lower atmosphere, where the pure rotation and the vibration-rotation bands of  $H_2O$  play a major role. Furthermore, the higher-state spectra are even important when considering the absorptivity or emissivity of water vapor at elevated temperature.

From  $250\text{ cm}^{-1}$  to  $4000\text{ cm}^{-1}$ , two absorption-free regions at room temperature remain yet to be properly filled by experimental investigations of steam; namely,  $2000\text{ cm}^{-1}$  to  $3000\text{ cm}^{-1}$  at the short wavelength end; and  $600\text{ cm}^{-1}$  to  $1250\text{ cm}^{-1}$  at the long wavelength end. This is the spectral range where spectrum originates from the higher energy levels of the molecule, which have a low population at room temperature. By raising the temperature of the water vapor molecule under investigation, Taylor, Benedict, and Strong, et al. started the observation

of highly excited state transitions.<sup>2-4</sup> Other pioneer studies at elevated temperature in one wavelength band or the other have been many.<sup>5-10</sup> Theoretical computation of spectral positions based on experimental results have been accomplished by Benedict and his associates.<sup>11,12</sup> Lines listed in References 11 and 12, having intensities greater than  $S = 0.0001 \text{ cm}^{-1}/(\text{gm}/\text{cm}^2)$  at  $287.7^\circ\text{K}$ , are more numerous than those which have been discovered in the laboratory. Our object in this investigation was to look for new bands and new lines in old bands in the spectrum of superheated steam using good resolution. The procedure we report here for the study of the temperature dependence of new band and line intensities should be particularly fruitful in analyzing other molecules, and should add to the detail and fineness of our knowledge of molecular structure.

Rock salt windows are not suitable for steam and no other window materials with good spectral transmission can stand a temperature as high as  $600^\circ\text{C}$ . Window covers of silver chloride for a conventional absorption cell reduced the energy excessively. Accordingly, to achieve good resolution we have used an absorption cell so adapted that it may be used without window covers. This improvement, made by eliminating window covers, is particularly important for some spectral regions because of the already low energy transmitted by the water vapor.

At elevated temperature water vapor molecules radiate enough energy at wavelength corresponding to the absorption lines that one may use the  $H_2O$  emission for spectral studies, and even for temperature determination. The superheated steam emissivities are equal to absorptivities, after Kirchhoff's law. Thus, the spectrum can be studied as both an absorption, or emission spectrum.<sup>18</sup> Studies of the emission of steam with resolving power sufficient to separate lines due to individual rotational transitions in these particular bands have not previously been reported.

#### HOT CELL AND OVERALL OPTICAL SYSTEM

The Pfund type hot cell used in this investigation, shown schematically in Fig. 1, consists of a steel tube of 3/8" thickness, 12" inner diameter and 51" overall length. It is heated to elevated temperature by means of 36 strip heaters (Chromalux, 500 watts, 120 volts) attached symmetrically in six separate banks around the outside of this steel tube. In addition, three element heaters (Chromalux, 250 watts, 120 volts) are mounted on the outside of each end plate. The whole cell with attached heaters is insulated with a layer of asbestos. This, in turn, is surrounded with five layers (almost 8 inches thick) of fiber glass. There is an air space of one to two inches between the outside of the cell and the asbestos. This arrangement permits

control of the temperature, and acts to minimize temperature gradients throughout the cell. Thermometers attached to the outside of the steel tube provide for monitoring the cell temperature change, but the working temperature of the steam is the average of thermometer readings taken inside along the axis of the cell.

Two gold-coated mirrors of 10-1/2" aperture, 1" thick and with a focal length of 41-11/16", each perforated with a 1-1/2" central hole, are mounted in the ends of the cell as shown in Fig. 1. Radiations from a Nernst glower transverse the cell, between  $M_1$  and  $M_2$ , three times, as indicated. The total absorption path for this triple-pass<sup>19</sup> absorption cell is 11-1/4 ft. Three adjustable lugs 120° apart from each other supporting the mirror mount are attached to the end plate of the cell and provide mechanisms so that optical alignment can be accomplished from outside the end plate when the cell is hot. The distance between the mirror surface and the end plate at room temperature is about 4-3/4".

The auxiliary mirror,  $M_3$ , transfers radiations from the Nernst glower to the cell's entrance opening. The flat mirror  $M_4$  and the  $LN_2$  filled Dewar flask are used as a background for emission studies. The spectrometer response measures the emission of the sample gas, since the liquid nitrogen emission is negligible.

$M_5$  and  $M_6$  form relay optics for final transfer of radiation from the emergence cell window onto the entrance slit of the  $f/4$  Perkin-Elmer spectrometer.  $M_6$ , an  $f/4$  spherical mirror, is used at its center of curvature. This relay optics has an air path of about 34" between the absorption cell and the spectrometer. It was, accordingly, covered with an aluminum box so that the room atmospheric carbon dioxide could be removed from the air path by purging the box continuously with dry tank nitrogen.

A water-cooled shielding plate was placed between the hot cell and the relay optics to prevent the diagonal mirror,  $M_5$ , from picking up ~~temperature~~ radiations from the end plate.

With this uncovered window hot cell the usual energy limitation on resolution was improved. During observation steam is introduced into the cell through two inlets in the center part of the cell and escapes through the small open windows at the two end plates.

#### OBSERVATION OF SPECTRA

A Perkin-Elmer Model 210B grating spectrometer was used in this investigation. It was flushed with a continuous flow of dry air (or with dry tank nitrogen, when it was scanning in the atmospheric carbon dioxide spectral region). The spectral components were detected by a thermocouple. Its output signal, amplified with

a Brower lock-in amplifier, was displayed by a Brown strip chart recorder. Spectra were recorded using the grating's first order, cut-on interference filters were used to reject higher orders of shorter wavelengths. The spectrometer was calibrated with standard spectral lines.<sup>13</sup> In the region from about  $2300\text{ cm}^{-1}$  to  $1975\text{ cm}^{-1}$  (Fig. 7) our assigned frequencies are based mainly on known water vapor lines and carbon monoxide lines observed with the same system--spectrometer and recorder.<sup>14</sup>

For absorption studies, mirror  $M_3$  and the Nernst glower were used. A water-cooled aluminum platform attached to the end plate of the heated cell, to secure optical stability, was used to support the auxiliary mirror  $M_3$ , the Nernst glower, and the chopper. In this instance the chopper was placed before the hot cell in order to avoid "seeing" the heated gases in the cell: although the emission of the heated gas falls on the detector, this emission does not give a response because the steam emission radiations were not synchronously chopped.

For emission observations, the mirror  $M_4$ , and cold source  $\text{LN}_2$  were placed in position. The chopper in this instance was installed after the hot cell. Since local cold source was not employed here, the chopper substitutes local dry air at room temperature for the distant cold source when the chopper blade interrupts the spectrometer's view of the distant source.

$M_1$  and  $M_2$ , after preliminary alignment at room temperature before heating, have to be readjusted at elevated temperature to correct for mirror changes caused by the steel tube expansion. This combination of  $M_1$  and  $M_2$  has two conjugate points at equal distance from the center of the cell. After the cell was heated to  $600^\circ\text{C}$ , and the temperature became stabilized, the light beam of the Nernst glower was refocused onto one of these conjugate points, and relay optics were readjusted to focus the spectrometer's entrance slit on the cell's other conjugate point. This effected a transference of maximum infrared energy from the Nernst source to the spectrometer. This alignment is essential for both emission and absorption studies. Finally, in the case of emission studies, the Nernst glower was removed and replaced by the  $\text{LN}_2$  background.

When recording spectra, a continuous stream of steam from a gently boiling flask of distilled and demineralized water entered into the heated cell and escaped through the windows at the two ends. The cell was filled with steam by displacement, at  $600^\circ\text{C}$ . A very slight increment of steam pressure, above atmosphere pressure, was maintained to prevent convection at the 1-1/2" windows. For mapping spectral areas of high absorption, in order to avoid line blending, the steam was shut off temporarily to obtain suitable concentrations

of water vapor. (cf. Fig. 10 and Table V).

Where atmospheric carbon dioxide absorption is high in the 14.986 micron region, the spectrometer, the chopper, and the aluminum box that contained the relay mirrors, were flushed by dry nitrogen. The unwanted natural  $\text{CO}_2$  component of the room air was almost but not completely removed from the 6.5 ft. air path. This would help much to differentiate pure  $\text{H}_2\text{O}$  lines from  $\text{CO}_2$  absorptions for this uncovered window cell.

### RESULTS AND DISCUSSIONS

In this work we searched for lines having such high energy levels that they are not observable at room temperature--lines lying in the spectral range from  $600\text{ cm}^{-1}$  to  $1250\text{ cm}^{-1}$ , and from  $2000\text{ cm}^{-1}$  to  $3000\text{ cm}^{-1}$ . In addition to  $600^\circ\text{C}$ , spectra were also measured at  $250^\circ\text{C}$ , and  $450^\circ\text{C}$  in the same range. The number of lines observed in the spectra at  $450^\circ\text{C}$  was found to be almost double those observed at  $250^\circ\text{C}$ ; even more weak lines become enhanced at  $600^\circ\text{C}$ .

We observed nearly 400 lines in the short wavelength range from  $3.29\mu$  to  $5.06\mu$ , and nearly 700 lines in the long wavelength range from  $7.91\mu$  to  $16.25\mu$ , all with good resolution. Figs. 2-11 show some of the superheated steam infrared spectra for the cell at  $600^\circ\text{C}$ , one atmosphere pressure. Except for Fig. 6, each figure

includes two curves in the same wavelength region, an emission spectrum appears above the absorption spectrum. Fig. 11 has two absorption spectra, representing different water vapor concentrations, below the steam emission spectrum at the top. A wavenumber scale at the bottom of the curve, and a vertical deflection scale are added to each figure for orientation purposes. A brief description of the salient feature of each figure is given on the accompanying pages.

The lines have been numbered in order of decreasing frequency in the figures as an aid to their identification in Tables II to V. For convenience, lines are grouped into four tables from Table II to Table V, according to the spectral gaps. The line number is given in the first column of the table and the observed frequency in the second. In the third column we add remarks. An index to the figures is presented here for reference. The effective spectral slit width at different frequencies appears in Table I.

The infrared spectra of superheated steam at 600°C from 2950  $\text{cm}^{-1}$  to 2750  $\text{cm}^{-1}$ , and from 2484  $\text{cm}^{-1}$  to 2380  $\text{cm}^{-1}$  are shown in Fig. 2, Fig. 3, and Fig. 4, respectively, which have been less thoroughly observed. There is an absorption-free region between 2750  $\text{cm}^{-1}$  to 2485  $\text{cm}^{-1}$ . We have observed many more lines than have been previously published, between 2240  $\text{cm}^{-1}$  and 2000  $\text{cm}^{-1}$ ,

## INDEX TO SPECTRA

<u>Figure</u>	<u>Spectral Region</u> <u>cm<sup>-1</sup></u>	<u>Grating</u> <u>1/mm</u>	<u>Conditions under which</u> <u>Spectra were obtained</u>
2	3035 2890	240	steam, 600°C
3	2890 2750	240	steam, 600°C
4	2470 2380	240	steam, 600°C
5	2300 1975	240	steam, 600°C
6	1260 1170	101	air, 600°C
7	1170 1060	101	steam, 600°C
8	1060 940	101	steam, 600°C
9	940 820	101	steam, 600°C
10	820 715	101	steam,* 600°C
11	715 615	101	steam, air, 600°C

\*Steam was shut off temporarily just before scanning to the strong absorption spectral area and turned on immediately after for the following weaker lines.

as depicted in Fig. 5.<sup>2,3</sup> These could interfere with the 4.66 $\mu$  band carbon monoxide lines, as applied to air pollution detection, if high temperature water vapor were present in the absorption path.<sup>14</sup> Many new lines were also observed in the region from 2240  $\text{cm}^{-1}$  to 2300  $\text{cm}^{-1}$ .

Figures 6 to 11 show the infrared spectra of superheated steam observed at 600°C from 1260  $\text{cm}^{-1}$  to 615  $\text{cm}^{-1}$ . Some lines that are observable at room temperature in this range become blending at 600°C. For the best display of water vapor spectra from 1260  $\text{cm}^{-1}$  to 1160  $\text{cm}^{-1}$  we filled in the heated cell with laboratory air. These spectra were depicted in Fig. 6. Similarly some lines in Fig. 10 are observable at room temperature and become high absorptions at 600°C. Here the steam was turned off as the scanning approaches a spectral area known from previous scanning to be opaque; and turned on as the scanning came out of the area. The purpose of this was to reveal the spectral structure in this area. The amount of steam involved is unknown. All these lines are remarked in Table V.

Water vapor lines were observed in the 14.986 $\mu$  carbon dioxide band region in spite of difficulties. One of these was carbon dioxide absorptions due to residual  $\text{CO}_2$  in the 6.5 ft. air path which was dry nitrogen flushed, but not completely. The other

difficulty was due to the high absorptions of water vapor at elevated temperature. We observed hot air absorptions at 600°C (humidity 79% at 82°F, typical Amherst air at the end of August) in addition to the steam absorptions and emissions in this wavelength region. Their spectra are depicted in Fig. 11. Each curve was obtained with the same spectrometer slit width: 0.377 mm. The middle curve is a mixture of water vapor absorptions and atmospheric carbon dioxide absorptions. The carbon dioxide spectrum is singled out and indicated by a downward arrow. Both natural carbon dioxide in the heated cell and in the 6.5 ft. air path would contribute to the  $\text{CO}_2$  absorption spectra. The top curve represents steam emissions; here water vapor emission lines are superimposed on the  $\text{CO}_2$  absorptions in the 6.5 ft. air path. The  $\text{CO}_2$  lines marked by asterisks in the top curve, are in good agreement in spectral positions with the downward arrow lines in the middle curve. In this manner the pure water vapor lines are identified. The  $\text{H}_2\text{O}$  line is indicated by a vertical dash in the middle curve, and an upward arrow in the top. Downward arrow lines between No. 28 ( $687.16 \text{ cm}^{-1}$ ) and No. 42 ( $667.82 \text{ cm}^{-1}$ ) appear to be nearly pure  $\text{CO}_2$  absorptions; those following line No. 61 ( $651.94 \text{ cm}^{-1}$ ) are probably due to absorptions other than  $\text{CO}_2$  because they exhibit high absorptions

in the superheated steam as shown in the bottom curve of Fig. 11. Other spectral lines marked with a downward arrow between line No. 42 and No. 61 could be  $\text{CO}_2$ , or  $\text{H}_2\text{O}$  lines, or both. Molecular identifications described here are not very satisfying, but perhaps the best which can be achieved with the information at present available.

The wavenumbers presented here are corrected to vacuum conditions. Line frequencies have been rounded off to the nearest  $0.01 \text{ cm}^{-1}$ . The recorded spectra have very good signal-to-noise ratio and spurious lines are not expected--except in some regions where absorption is weak as shown in the end of Fig. 3. But in this region, the absorption spectrum is confirmed by the corresponding emission line in the top curve. Serious ambiguities were avoided, due to either the instrument noise or steam fluctuations, by scanning each spectral range for two to three times--weak absorption lines are confirmed by coincidences.

Spectral positions reported in Table II-V have been compared to those tabulated by Benedict, et al.<sup>4,5</sup> Most lines are in good agreement with reasonable errors, especially the strong absorption lines observed in the superheated steam. In the above reference, there is a lower limit ( $700 \text{ cm}^{-1}$ ) to the theoretical predictions

for the  $6.3\mu$  band.<sup>5</sup> Our observed steam lines extend beyond this limit to  $615\text{ cm}^{-1}$ . From  $1150\text{ cm}^{-1}$  to  $700\text{ cm}^{-1}$  there are many more observed steam spectra than those predicted. Some of our observed lines from  $1050\text{ cm}^{-1}$  to  $615\text{ cm}^{-1}$  must originate from even highly excited state transitions which have room temperature intensities less than or equal to  $0.0001\text{ cm}^{-1}/\text{gm}/\text{cm}^2$ . On the other hand, listed in the same table for the  $6.3\mu$  band, some slight water vapor ( $\text{HHO}^{16}$ ) lines having room temperature intensities of  $10^{-4}\text{ cm}^{-1}/\text{gm}/\text{cm}^2$  were found falling in the absorption-free region ( $2750\text{ cm}^{-1} - 2470\text{ cm}^{-1}$ ) at  $600^\circ\text{C}$ .

The natural isotopes of water molecules  $\text{HHO}^{16}$ ,  $\text{HHO}^{18}$ ,  $\text{HHO}^{17}$ , and  $\text{HDO}^{16}$  have normal abundances of 99.73, 0.2039, 0.0373, and 0.0298 respectively.<sup>15</sup> The  $\nu_1$  fundamental band of HDO has been observed, resolved at  $3.67\mu$ .<sup>16,17</sup> It seems that we can conclude that the very small natural abundance of HDO fails to produce infrared spectrum around  $2720\text{ cm}^{-1}$  at  $600^\circ\text{C}$ . If so, the probabilities for molecule HDO of natural abundance to contribute spectra in other wavelength ranges would be small, not to mention their intrinsic weak absorptions that could have been masked by  $\text{HHO}^{16}$  in the  $\nu_2$  band.

$\text{H}_2\text{O}$  emission spectra at  $600^\circ\text{C}$  have been obtained with almost the same spectrometer slit width as used

for absorptions in each spectral region. Due to the great increase in resolving power of this system, we can now obtain emission spectra showing very much more detail. It may provide information for the calculation of the emissivity of flames and a knowledge of high temperature emission spectra may also facilitate the interpretation of flame and explosion spectra to determine combustion products.

#### ACKNOWLEDGEMENT

The author wishes to express his appreciation to Professor John D. Strong who has not only been endlessly available for consultation, and collaborated in solving the more difficult experimental problems in this work, but also has been a source of inspiration throughout the entire program. Thanks are due to the entire staff of the Astronomy Research Facility, especially to Mr. William S. Dalton, and Mr. Ta-Chun Li, for their generous assistance in carrying out, and completing this research. This work was partially financed by ARPA Contract F19628-70-C-0296 and ARPA Contract F19628-72-C-0075. Thanks are also extended to the United States-China Cooperative Science Program.

TABLE I  
EFFECTIVE SLITWIDTH

Wavenumber, $\text{cm}^{-1}$	Slitwidth, mm	Slitwidth, $\text{cm}^{-1}$
3030.00	.051	.82
3010.00	.051	.81
2990.00	.051	.80
2850.00	.068	.93
2800.00	.068	.89
2750.00	.068	.86
2480.00	.085	.84
2450.00	.085	.82
2420.00	.085	.79
2390.00	.085	.77
2300.00	.084	.71
2200.00	.084	.64
2100.00	.084	.59
2000.00	.084	.52
1900.00	.084	.46
1260.00	.095	.67
1240.00	.095	.65
1220.00	.095	.63
1200.00	.095	.61
1180.00	.095	.59
1160.00	.095	.57
1140.00	.095	.55
1120.00	.095	.53
1100.00	.095	.51
1080.00	.095	.49
1060.00	.125	.59
1040.00	.125	.56
1020.00	.125	.54
1000.00	.125	.52

TABLE I  
(Continued)

Wavenumber, $\text{cm}^{-1}$	Slitwidth, mm	Slitwidth, $\text{cm}^{-1}$
980.00	.125	.50
960.00	.167	.60
940.00	.167	.57
920.00	.167	.55
900.00	.167	.52
880.00	.167	.50
860.00	.202	.55
840.00	.202	.52
820.00	.272	.63
800.00	.272	.59
780.00	.272	.56
760.00	.272	.52
740.00	.272	.49
720.00	.272	.46
700.00	.377	.56
680.00	.377	.51
660.00	.377	.47
640.00	.377	.43
620.00	.377	.36

TABLE II  
 WATER VAPOR SPECTRUM AT 600°C  
 AND ONE ATMOSPHERE PRESSURE BETWEEN  
 3.29 $\mu$  AND 3.63 $\mu$

Line Number	Observed Wavenumber, cm <sup>-1</sup>	Remarks
Fig. 2, 1	3035.89	
2	3034.27	*
3	3031.74	*
4	3030.79	*
5	3028.69	
6	3028.04	
7	3025.78	*
8	3023.65	
9	3022.76	*
10	3018.97	
11	3015.56	*
12	3012.44	
13	3010.30	*
14	3008.54	
15	3004.68	
16	3003.89	*
17	3001.47	
18	3001.04	
19	2999.18	
20	2997.25	
21	2993.58	
22	2991.77	*
23	2987.42	*
24	2983.51	
25	2982.10	
26	2980.35	*
27	2977.40	
28	2974.60	
29	2973.22	*
30	2971.21	

TABLE II  
(Continued)

<u>Line Number</u>	<u>Observed Wavenumber, cm<sup>-1</sup></u>	<u>Remarks</u>
Fig. 2, 31	2969.35	
32	2967.44	
33	2966.70	
34	2965.92	
35	2964.08	
36	2961.28	
37	2958.12	*
38	2956.21	
39	2955.56	*
40	2953.94	
41	2951.39	
42	2948.79	
43	2946.56	
44	2945.99	
45	2944.53	
46	2943.41	
47	2941.61	
48	2939.79	
49	2936.99	
50	2935.25	
51	2933.15	
52	2929.66	
53	2928.90	
54	2927.60	
55	2925.96	
56	2924.77	
57	2922.57	
58	2921.44	
59	2920.37	
60	2918.96	
61	2916.07	
62	2915.37	
63	2914.41	

TABLE II  
(Continued)

Line Number	Observed Wavenumber, $\text{cm}^{-1}$	Remarks
Fig. 2, 64	2911.61	
65	2909.55	
66	2908.42	
67	2906.71	
68	2905.69	
Fig. 2, 69; Fig. 3, 1	2904.42	
70;	2901.77	
71;	2899.42	
72;	2396.72	
73;	2895.48	
74;	2893.05	
75;	2891.95	
76;	2890.37	
77;	2887.94	
10	2885.90	
11	2882.76	
12	2881.50	
13	2877.53	
14	2875.96	
15	2874.87	
16	2871.13	
17	2868.47	
18	2866.21	
19	2862.96	
20	2862.09	
21	2859.87	
22	2858.36	
23	2857.15	
24	2855.16	
25	2853.96	
26	2851.81	
27	2849.65	
28	2847.41	
29	2846.69	

TABLE II  
(Continued)

Line Number	Observed Wavenumber, $\text{cm}^{-1}$	Remarks
Fig. 3, 30	2844.99	
31	2842.47	
32	2840.92	
33	2839.24	
34	2833.69	
35	2830.69	
36	2828.64	
37	2826.17	
38	2825.21	
39	2824.13	
40	2822.07	
41	2820.32	
42	2818.29	
43	2817.17	
44	2814.05	
45	2812.03	
46	2809.00	
47	2806.26	
48	2803.80	
49	2801.16	
50	2798.84	
51	2797.32	
52	2795.11	
53	2778.11	
54	2775.40	
55	2769.03	
56	2766.09	
57	2763.49	
58	2757.46	
59	2754.68	
60	2752.25	

\*Line observable at room temperature!

TABLE III

WATER VAPOR SPECTRUM AT 600°C  
AND ONE ATMOSPHERE PRESSURE BETWEEN  
4.03 $\mu$  AND 4.20 $\mu$

Line Number	Observed Wavenumber, $\text{cm}^{-1}$	Remarks
Fig. 4, 1	2484.62	
2	2483.40	
3	2474.96	
4	2473.09	
5	2471.36	
6	2469.35	
7	2467.44	
8	2465.03	
9	2463.11	
10	2461.28	
11	2459.42	
12	2453.40	
13	2448.89	
14	2447.29	
15	2444.47	
16	2442.78	
17	2440.82	
18	2437.60	
19	2435.13	
20	2432.86	
21	2430.00	
22	2428.71	
23	2427.13	
24	2425.23	
25	2422.93	
26	2421.83	
27	2420.17	
28	2416.61	
29	2415.48	
30	2412.89	

TABLE III  
(Continued)

Line Number	Observed Wavenumber, $\text{cm}^{-1}$	Remarks
Fig. 4, 31	2411.66	
32	2409.16	
33	2407.57	
34	2405.96	
35	2402.38	
36	2400.74	
37	2397.45	
38	2396.84	
39	2395.21	
40	2393.70	
41	2391.04	
42	2389.52	
43	2388.51	
44	2387.19	
45	2386.65	
46	2386.15	
47	2384.54	
48	2381.59	
49	2380.51	

TABLE IV  
WATER VAPOR SPECTRUM AT 600°C  
AND ONE ATMOSPHERE PRESSURE BETWEEN  
4.35 $\mu$  AND 5.06 $\mu$

Line Number	Observed Wavenumber, $\text{cm}^{-1}$	Remarks
Fig. 5, 1	2300.77	
2	2299.99	
3	2299.02	
4	2297.86	
5	2296.63	
6	2295.93	
7	2293.89	
8	2292.72	
9	2291.86	
10	2290.25	
11	2289.69	
12	2288.49	
13	2287.34	
14	2286.68	
15	2285.44	
16	2284.95	
17	2283.83	
18	2282.38	
19	2281.57	
20	2281.28	
21	2280.11	
22	2278.94	
23	2277.48	
24	2276.88	
25	2275.35	
26	2274.68	

TABLE IV  
(Continued)

Line Number	Observed Wavenumber, $\text{cm}^{-1}$	Remarks
Fig. 5, 57	2238.28	
58	2235.41	
59	2233.38	
60	2231.12	
61	2230.38	
62	2227.42	
63	2226.24	
64	2225.88	
65	2224.08	
66	2222.06	
67	2221.11	
68	2218.57	
69	2215.81	
70	2214.32	
71	2213.36	
72	2211.56	
73	2210.07	
74	2209.07	
75	2206.18	
76	2205.35	
77	2203.88	
78	2202.09	
79	2200.36	
80	2198.56	
81	2196.66	
82	2195.20	
83	2194.28	
84	2192.99	
85	2191.63	
86	2190.40	

TABLE IV  
(Continued)

Line Number	Observed Wavenumber, $\text{cm}^{-1}$	Remarks
Fig. 5, 87	2189.51	
88	2186.86	
89	2185.26	
90	2183.64	
91	2182.93	
92	2181.40	
93	2179.08	
94	2177.05	
95	2175.11	
96	2172.18	
97	2171.13	
98	2169.05	
99	2166.54	
100	2164.68	
101	2162.75	
102	2161.33	
103	2160.68	
104	2157.64	
105	2156.60	
106	2154.35	
107	2152.56	
108	2151.26	
109	2148.22	
110	2147.56	
111	2144.99	
112	2141.55	
113	2139.35	
114	2138.26	
115	2136.20	
116	2135.58	

TABLE IV  
(Continued)

<u>Line Number</u>	<u>Observed Wavenumber, cm<sup>-1</sup></u>	<u>Remarks</u>
Fig. 5, 117	2131.50	
118	2129.41	
119	2128.46	
120	2127.29	
121	2126.12	
122	2124.03	
123	2122.51	
124	2121.70	
125	2119.32	
126	2118.51	
127	2115.25	
128	2114.38	
129	2111.85	
130	2110.54	
131	2109.45	
132	2107.52	
133	2104.52	
134	2103.38	
135	2100.52	
136	2097.21	
137	2094.90	
138	2093.36	
139	2092.23	
140	2090.09	
141	2087.41	
142	2085.82	
143	2083.27	
144	2081.94	
145	2079.97	
146	2078.50	
147	2076.73	
148	2075.64	

TABLE IV  
(Continued)

Line Number	Observed Wavenumber, $\text{cm}^{-1}$	Remarks
Fig. 5, 149	2074.37	
150	2072.02	
151	2070.46	
152	2068.65	
153	2067.88	
154	2067.06	
155	2065.84	
156	2064.85	
157	2062.66	
158	2060.50	
159	2058.81	
160	2057.56	
161	2055.95	
162	2053.85	
163	2051.19	
164	2048.50	
165	2047.75	
166	2046.58	
167	2043.95	*
168	2041.43	*
169	2039.55	
170	2037.51	*
171	2035.44	
172	2034.10	*
173	2032.00	
174	2030.56	
175	2028.54	
176	2026.59	*
177	2023.36	*
178	2021.71	
179	2019.87	

TABLE IV  
(Continued)

Line Number	Observed Wavenumber, $\text{cm}^{-1}$	Remarks
Fig. 5, 180	2019.25	
181	2018.55	*
182	2016.80	*
183	2015.20	
184	2014.37	
185	2012.28	
186	2010.88	
187	2009.33	*
188	2007.74	*
189	2005.62	
190	2004.39	
191	2003.45	
192	2000.97	
193	1998.98	*
194	1996.69	
195	1995.05	
196	1993.26	*
197	1991.86	
198	1988.97	*
199	1987.37	
200	1985.15	
201	1982.09	
202	1979.70	
203	1978.43	
204	1976.19	*
205	1975.42	
206	1973.04	

\*Line observable at room temperature!

TABLE V

WATER VAPOR SPECTRUM AT 600°C  
AND ONE ATMOSPHERE PRESSURE BETWEEN  
7.91 $\mu$  AND 16.25 $\mu$

Line Number	Observed Wavenumbers, $\text{cm}^{-1}$	Remarks
Fig. 6, 1	1263.93	*
2	1263.57	
3	1262.03	
4	1260.37	*, &
5	1258.67	*, &
6	1256.57	&
7	1255.86	
8	1254.54	
9	1254.21	
10	1253.71	
11	1253.37	
12	1252.99	
13	1252.46	
14	1251.87	
15	1251.33	
16	1250.97	
17	1250.53	
18	1249.83	
19	1249.55	
20	1249.08	
21	1248.30	
22	1247.02	
23	1246.48	
24	1246.09	
25	1245.14	
26	1244.88	
27	1244.49	

TABLE V  
(Continued)

Line Number	Observed Wavenumber, $\text{cm}^{-1}$	Remarks
Fig. 6, 28	1244.28	*, &
29	1243.04	&
30	1242.59	
31	1241.49	
32	1241.04	
33	1239.26	&
34	1238.48	
35	1238.24	
36	1237.75	
37	1237.38	
38	1237.03	
40	1236.19	
41	1235.38	
42	1234.95	
43	1234.41	
44	1233.24	
45	1232.50	
46	1231.93	
47	1231.68	
48	1230.48	
49	1229.63	
50	1229.23	
51	1228.34	
52	1228.12	
53	1227.05	
54	1226.63	
55	1226.40	
56	1225.48	*, &
57	1225.10	
58	1224.94	&
59	1224.11	
60	1223.74	
61	1223.29	
62	1221.82	

TABLE V  
(Continued)

Line Number	Observed Wavenumber, $\text{cm}^{-1}$	Remarks
Fig. 6, 63	1221.49	
64	1221.21	
65	1220.04	&
66	1219.41	
67	1217.68	
68	1217.44	
69	1216.28	
70	1215.98	
71	1215.71	
72	1214.32	
73	1214.21	
74	1213.89	
75	1213.03	
76	1212.75	
77	1212.34	*, &
78	1211.06	*, &
79	1209.35	
80	1208.68	
81	1207.59	
82	1206.80	
83	1206.23	
84	1205.56	
85	1203.48	
86	1201.28	
87	1200.99	
88	1200.55	&
89	1200.07	
90	1199.72	
91	1198.89	
92	1198.26	*, &
93	1197.10	
94	1196.66	

TABLE V  
(Continued)

Line Number	Observed Wavenumber, $\text{cm}^{-1}$	Remarks
Fig. 6 , 95	1195.19	
96	1193.90	
97	1193.49	
98	1192.54	
99	1191.89	
100	1191.29	
101	1190.39	
102	1189.92	
103	1189.53	
104	1188.20	
105	1186.95	*,&
106	1185.41	
107	1185.10	
108	1184.35	
109	1183.73	
110	1183.40	
111	1182.93	
112	1182.70	
113	1179.49	
114	1179.03	
115	1178.54	
116	1177.81	
117	1177.43	
118	1176.43	
119	1174.58	*,&
120	1173.43	
121	1172.69	
122	1172.30	
123	1171.54	

TABLE V  
(Continued)

Line Number				Observed Wavenumber, $\text{cm}^{-1}$	Remarks
Fig. 6 ,	124;	Fig. 7 ,	1	1169.87	
	125;		2	1167.87	
	126;		3	1167.48	
	127;		4	1166.14	
	128;		5	1165.16	
	129;		6	1163.87	
	130;		7	1162.74	
	131;		8	1160.09	
			9	1158.77	
			10	1158.15	
			11	1156.96	
			12	1156.18	
			13	1155.11	
			14	1153.96	
			15	1153.37	
			16	1152.43	*
			17	1151.55	
			18	1151.19	
			19	1149.48	*
			20	1148.25	
			21	1146.67	
			22	1144.96	
			23	1143.62	
			24	1142.88	
			25	1141.56	
			26	1139.18	
			27	1138.58	
			28	1137.37	*
			29	1136.93	
			30	1136.44	
			31	1135.96	*
			32	1135.75	*
			33	1134.88	

TABLE V  
(Continued)

Line Number	Observed Wavenumber, $\text{cm}^{-1}$	Remarks
Fig. 7, 34	1134.57	
35	1133.51	
36	1132.79	
37	1131.95	
38	1130.52	
39	1130.10	
40	1129.08	
41	1128.61	
42	1128.05	
43	1126.62	
44	1125.39	
45	1123.31	
46	1123.15	
47	1122.99	
48	1121.30	*
49	1120.87	
50	1119.30	
51	1118.94	
52	1117.95	
53	1117.61	
54	1116.45	
55	1115.36	
56	1114.59	
57	1113.45	
58	1112.36	
59	1111.69	*
60	1109.99	
61	1107.91	
62	1106.76	*
63	1106.36	
64	1105.10	
65	1104.56	
66	1103.80	
67	1103.03	

TABLE V  
(Continued)

Line Number	Observed Wavenumber, $\text{cm}^{-1}$	Remarks
Fig. 7, 68	1101.54	
69	1099.64	
70	1097.85	
71	1097.48	
72	1097.20	
73	1096.33	
74	1095.75	
75	1094.39	
76	1093.75	
77	1093.10	
78	1092.45	
79	1091.65	
80	1091.23	
81	1090.58	
82	1089.73	
83	1089.28	
84	1088.72	
85	1087.96	
86	1087.17	
87	1086.91	
88	1086.31	
89	1085.67	
90	1085.44	
91	1084.97	
92	1083.77	
93	1082.10	
94	1081.38	
95	1080.51	
96	1079.92	
97	1079.58	
98	1079.26	
99	1078.60	
100	1077.56	

TABLE V  
(Continued)

Line Number	Observed Wavenumber, $\text{cm}^{-1}$	Remarks
Fig. 7, 101	1076.79	
102	1076.11	
103	1075.51	
104	1074.21	
105	1074.23	
106	1072.63	
107	1071.44	
108	1069.94	
109	1068.87	
110	1068.23	
111	1067.93	
112	1066.73	
113	1066.08	
114	1064.76	
115	1063.84	
116	1063.49	
117	1062.66	
118	1061.16	
119	1060.70	
Fig. 7, 120; Fig. 8, 1	1060.15	
121; 2	1059.50	
122; 3	1058.16	
123; 4	1057.54	
5	1055.56	
6	1054.94	
7	1053.87	
8	1053.57	
9	1052.22	
10	1051.71	
11	1050.25	
12	1049.45	
13	1048.09	

TABLE V  
(Continued)

Line Number	Observed Wavenumber, $\text{cm}^{-1}$	Remarks
Fig. 8, 14	1047.66	
15	1046.63	
16	1045.81	
17	1044.47	
18	1042.50	
19	1040.91	
20	1039.47	
21	1038.90	
22	1038.10	
23	1035.96	
24	1034.28	
25	1032.82	
26	1031.46	
27	1029.43	
28	1028.63	
29	1028.10	
30	1025.58	
31	1024.98	
32	1023.14	
33	1022.14	
34	1021.15	
35	1019.87	
36	1019.01	
37	1017.90	
38	1016.81	
39	1014.67	
40	1013.63	
41	1011.56	
42	1010.75	
43	1009.96	
44	1008.99	
45	1007.55	

TABLE V  
(Continued)

Line Number	Observed Wavenumber, $\text{cm}^{-1}$	Remarks
Fig. 8, 46	1006.70	
47	1004.50	
48	1003.80	
49	1003.19	
50	1002.41	
51	1001.33	
52	1000.33	
53	1000.10	
54	998.46	
55	997.44	
56	995.77	
57	995.39	
58	994.27	
59	992.92	
60	992.13	
61	990.47	
62	990.09	
63	988.60	
64	987.26	
65	985.06	
66	983.71	
67	982.81	
68	981.17	
69	978.59	
70	977.50	
71	975.73	
72	973.07	
73	971.63	
74	970.49	
75	969.05	
76	968.02	
77	967.62	
78	967.01	

TABLE V  
(Continued)

Line Number	Observed Wavenumber, $\text{cm}^{-1}$	Remarks
Fig. 8, 79	965.91	
80	965.23	
81	964.85	
82	963.37	
83	963.06	
84	961.96	
85	960.82	
86	960.56	
87	959.17	
88	958.07	
89	956.66	
90	955.78	
91	954.15	
92	953.35	
93	951.95	
94	951.49	
95	949.49	
96	948.23	
97	947.29	
98	947.05	
99	946.30	
100	945.63	
101	944.87	
102	944.03	
103	943.29	
104	942.09	
105	941.11	
Fig. 9, 1	940.41	
2	939.60	
3	939.10	
4	938.88	
5	938.04	

TABLE V  
(Continued)

Line Number	Observed Wavenumber, $\text{cm}^{-1}$	Remarks
Fig. 9, 6	935.99	
7	935.01	
8	933.69	
9	933.06	
10	930.39	
11	928.94	
12	927.76	
13	926.36	
14	926.04	
15	924.89	
16	923.81	
17	922.47	
18	922.15	
19	921.71	
20	919.88	
21	918.83	
22	917.85	
23	917.04	
24	915.97	
25	914.47	
26	914.06	
27	912.66	
28	910.76	
29	910.17	
30	909.47	
31	909.06	
32	908.75	
33	907.81	
34	906.39	
35	906.09	
36	905.54	
37	904.65	
38	903.40	

TABLE V  
(Continued)

Line Number	Observed Wavenumber, $\text{cm}^{-1}$	Remarks
Fig. 9, 39	902.23	
40	901.27	
41	900.84	
42	900.46	
43	899.22	
44	897.65	
45	896.40	
46	895.60	
47	894.60	
48	892.89	
49	892.49	
50	891.28	
51	890.13	
52	888.71	
53	887.68	
54	887.25	
55	885.64	
56	884.84	
57	883.18	
58	880.05	
59	878.61	
60	877.46	
61	877.03	
62	874.99	
63	874.23	
64	872.96	
65	871.31	
66	870.16	
67	868.03	
68	866.99	
69	865.92	
70	865.27	

TABLE V  
(Continued)

Line Number	Observed Wavenumber, $\text{cm}^{-1}$	Remarks
Fig. 9 , 71	864.33	
72	863.01	
73	861.92	
74	860.67	
75	859.70	
76	858.56	
77	856.73	
78	856.43	
79	856.02	
80	855.57	
81	854.47	*
82	852.76	*
83	852.09	
84	851.06	
85	849.58	*
86	848.72	
87	847.56	
88	847.05	
89	845.77	
90	843.45	
91	843.06	
92	842.11	
93	841.97	
94	841.18	
95	840.38	
96	840.03	
97	838.28	
98	837.95	
99	835.64	
100	833.77	
101	832.81	
102	831.18	

TABLE V  
(Continued)

Line Number	Observed Wavenumber, $\text{cm}^{-1}$	Remark
Fig. 9 , 103	830.68	
104	829.57	
105	828.66	
106	827.43	
107	826.20	
108	825.87	
109	825.58	
110	824.74	
111	824.00	
112	823.53	
113	822.73	
114	822.27	
115	820.55	
Fig. 9 , 116; Fig. 10, 1	819.44	
117; 2	818.21	
3	816.21	
4	815.04	
5	814.51	*,&
6	813.89	
7	813.63	
8	812.22	
9	811.46	
10	810.26	
11	809.70	
12	808.59	
13	808.35	&
14	807.13	
15	806.68	
16	806.40	
17	805.41	
18	803.71	*,&
19	803.03	

TABLE V  
(Continued)

Line Number	Observed Wavenumber, $\text{cm}^{-1}$	Remarks
Fig. 10, 20	802.59	
21	801.75	
22	800.93	
23	800.49	
24	799.32	
25	798.88	
26	797.84	*, &
27	796.86	
28	796.28	
29	795.05	*, &
30	794.10	
31	792.24	
32	791.93	
33	790.34	
34	789.46	
35	788.63	
36	787.59	
37	786.52	
38	785.70	
39	784.53	
40	784.05	*, &
41	783.48	
42	783.01	
43	782.71	
44	782.02	
45	780.49	
46	779.37	
47	779.01	
48	778.29	
49	777.14	*, &

TABLE V  
(Continued)

Line Number	Observed Wavenumber, $\text{cm}^{-1}$	Remarks
Fig. 10, 50	775.69	*, &
51.	774.63	
52	774.06	
53	772.61	
54	772.01	
55.	771.69	
56	770.18	&
57	769.15	
58	767.99	
59	767.59	
60	767.21	
61	766.28	
62	764.90	
63	763.56	
64	762.78	
65	762.05	
66	761.68	
67	761.37	
68	760.53	
69	758.91	
70	757.75	
71	756.95	
72	756.40	
73	756.16	&
74	755.88	
75	755.00	&
76	754.33	*, &
77	753.06	
78	752.54	&
79	751.34	
80	750.43	
81	748.73	
82	747.68	

TABLE V  
(Continued)

Line Number	Observed Wavenumber, $\text{cm}^{-1}$	Remarks
Fig. 10, 83	746.87	
84	745.19	
85	744.65	*,&
86	743.81	
87	742.52	
88	741.94	
89	740.98	
90	739.08	
91	738.27	
92	737.09	
93	736.26	
94	735.31	
95	734.27	
96	733.63	
97	732.80	
98	731.96	
99	730.77	
100	729.57	
101	728.68	
102	726.66	
103	726.35	
104	724.36	
105	723.41	
106	722.64	
107	721.83	
108	721.52	
109	720.42	
110	719.71	
111	718.83	
112	718.01	
113	716.68	
114	715.51	

TABLE V  
(Continued)

Line Number	Observed Wavenumber, $\text{cm}^{-1}$	Remarks
Fig. 10, 115; Fig. 11, 1	715.20	
2	714.02	
3	711.80	
4	710.02	
5	708.34	
6	707.34	
7	706.46	
8	705.33	
9	703.63	
10	702.16	
11	701.64	
12	700.16	
13	698.95	
14	698.58	
15	697.73	
16	697.10	
17	695.26	$\text{CO}_2/\text{H}_2$
18	694.18	
19	693.24	
20	691.98	$\text{CO}_2/\text{H}_2$
21	690.94	
22	690.64	
23	690.37	$\text{CO}_2/\text{H}_2$
24	690.03	
25	688.78	$\text{CO}_2/\text{H}_2$
26	688.12	
27	687.73	
28	687.16	$\text{CO}_2$
29	685.55	$\text{CO}_2$
30	683.96	$\text{CO}_2$
31	682.37	$\text{CO}_2$
32	680.78	$\text{CO}_2$

TABLE V  
(Continued)

Line Number	Observed Wavenumber, $\text{cm}^{-1}$	Remarks
Fig. 11, 33	679.20	$\text{CO}_2$
34	677.60	$\text{CO}_2$
35	676.04	$\text{CO}_2$
36	675.40	$\text{CO}_2$
37	674.45	$\text{CO}_2$
38	674.21	$\text{CO}_2$
39	672.88	$\text{CO}_2$
40	671.34	$\text{CO}_2$
41	688.54	$\text{CO}_2$
42	667.82	$\text{CO}_2$
43	666.62	$\text{CO}_2$
44	664.57	
45	664.08	
46	662.71	$\text{CO}_2/\text{H}_2\text{O}$
47	661.93	
48	661.17	$\text{CO}_2/\text{H}_2\text{O}$
49	660.25	
50	659.06	$\text{CO}_2/\text{H}_2\text{O}$
51	658.66	
52	658.36	
53	658.07	$\text{CO}_2/\text{H}_2\text{O}$
54	656.53	$\text{CO}_2/\text{H}_2\text{O}$
55	655.59	
56	655.06	$\text{CO}_2/\text{H}_2\text{O}$
57	653.85	
58	653.48	$\text{CO}_2/\text{H}_2\text{O}$
59	652.75	
60	652.37	
61	651.94	$\text{CO}_2/\text{H}_2\text{O}^{\$}$
62	650.40	$\text{CO}_2/\text{H}_2\text{O}^{\$}$
63	649.39	

TABLE V  
(Continued)

Line Number	Observed Wavenumber, $\text{cm}^{-1}$	Remarks
Fig. 11, 64	648.90	$\text{CO}_2/\text{H}_2\text{O}$
65	648.33	
66	647.39	$\text{CO}_2/\text{H}_2\text{O}$
67	645.90	$\text{CO}_2/\text{H}_2\text{O}$
68	645.45	
69	644.39	$\text{CO}_2/\text{H}_2\text{O}$
70	642.86	$\text{CO}_2/\text{H}_2\text{O}$
71	642.11	
72	641.37	$\text{CO}_2/\text{H}_2\text{O}$
73	639.83	$\text{CO}_2/\text{H}_2\text{O}$
74	639.36	
75	638.34	$\text{CO}_2/\text{H}_2\text{O}$
76	636.87	$\text{CO}_2/\text{H}_2\text{O}$
77	635.38	$\text{CO}_2/\text{H}_2\text{O}$
78	635.07	
79	634.37	
80	633.55	
81	632.66	
82	631.94	
83	631.21	
84	630.03	
85	628.41	
86	627.48	
87	625.95	*
88	625.01	
89	624.31	
90	622.51	
91	621.61	
92	620.02	*
93	619.15	
94	617.38	
95	616.78	
96	615.77	
97	615.37	

TABLE V  
(Continued)

\* Line observable at room temperature!

& Line in high absorption area.

CO<sub>2</sub> Believed to be pure atmosphere carbon dioxide absorptions picked up in the 6.5 ft. air path.

CO<sub>2</sub>/H<sub>2</sub>O Either CO<sub>2</sub> absorption or H<sub>2</sub>O absorption, or both.

CO<sub>2</sub>/H<sub>2</sub>O<sup>\$</sup> More likely due to H<sub>2</sub>O absorption than CO<sub>2</sub> absorption.

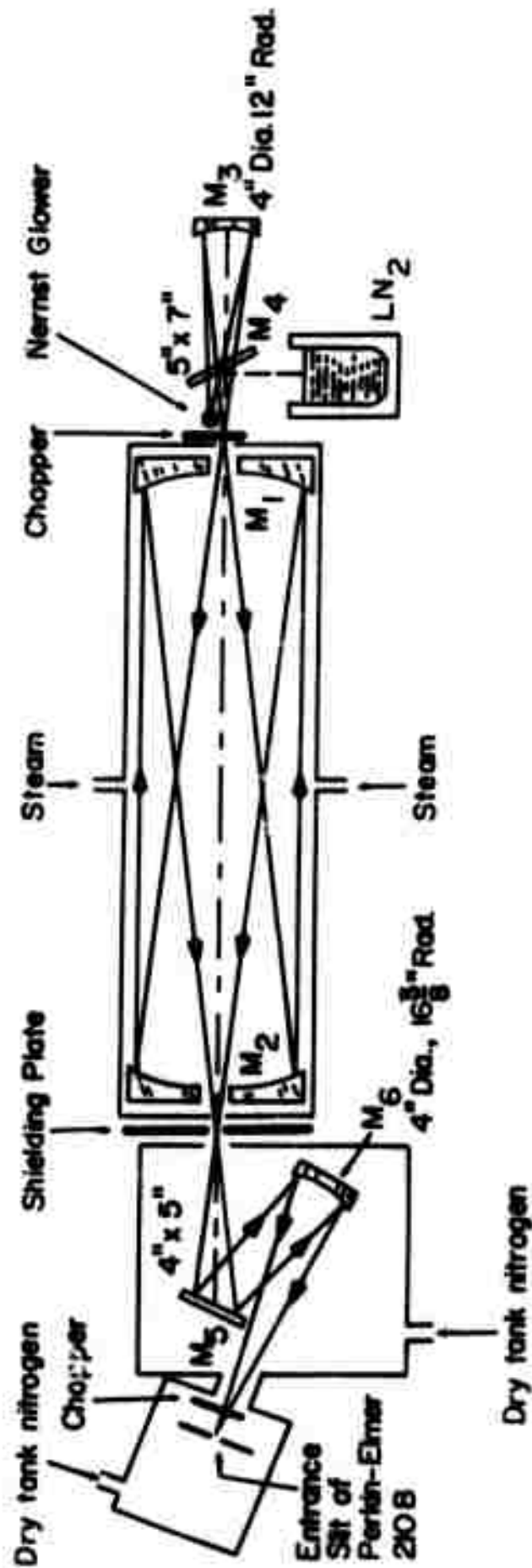


Fig. 1. Schematic drawing of the hot cell and overall optical set-up. Absorption studies are obtained when chopper is installed before the hot cell, mirror M<sub>4</sub> and cold source LN<sub>2</sub> are removed. For emission observations the chopper is placed after the hot cell, mirror M<sub>3</sub> and nernst glower are removed.

Fig. 3. Absorption and emission spectrum from 2890  $\text{cm}^{-1}$  to 2750  $\text{cm}^{-1}$  ( $3.46\mu$ - $3.63\mu$ ) of an 11-1/4 ft. path of steam at 600°C and one atmosphere pressure.

Fig. 2. Absorption and emission spectrum from 3035  $\text{cm}^{-1}$  to 2890  $\text{cm}^{-1}$  ( $3.29\mu$ - $3.46\mu$ ) of an 11-1/4 ft. path of steam at 600°C and one atmosphere pressure.

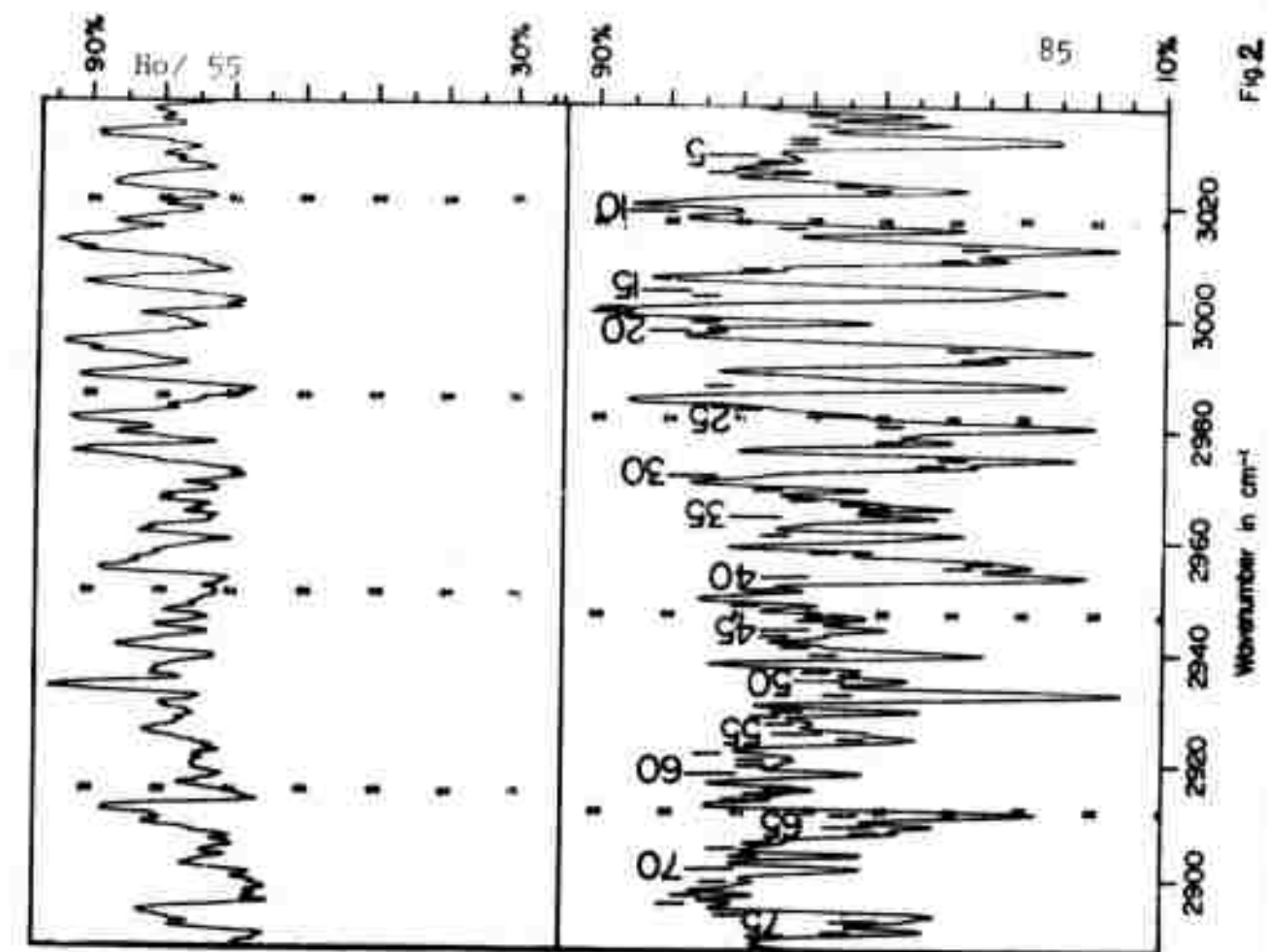


Fig 2.

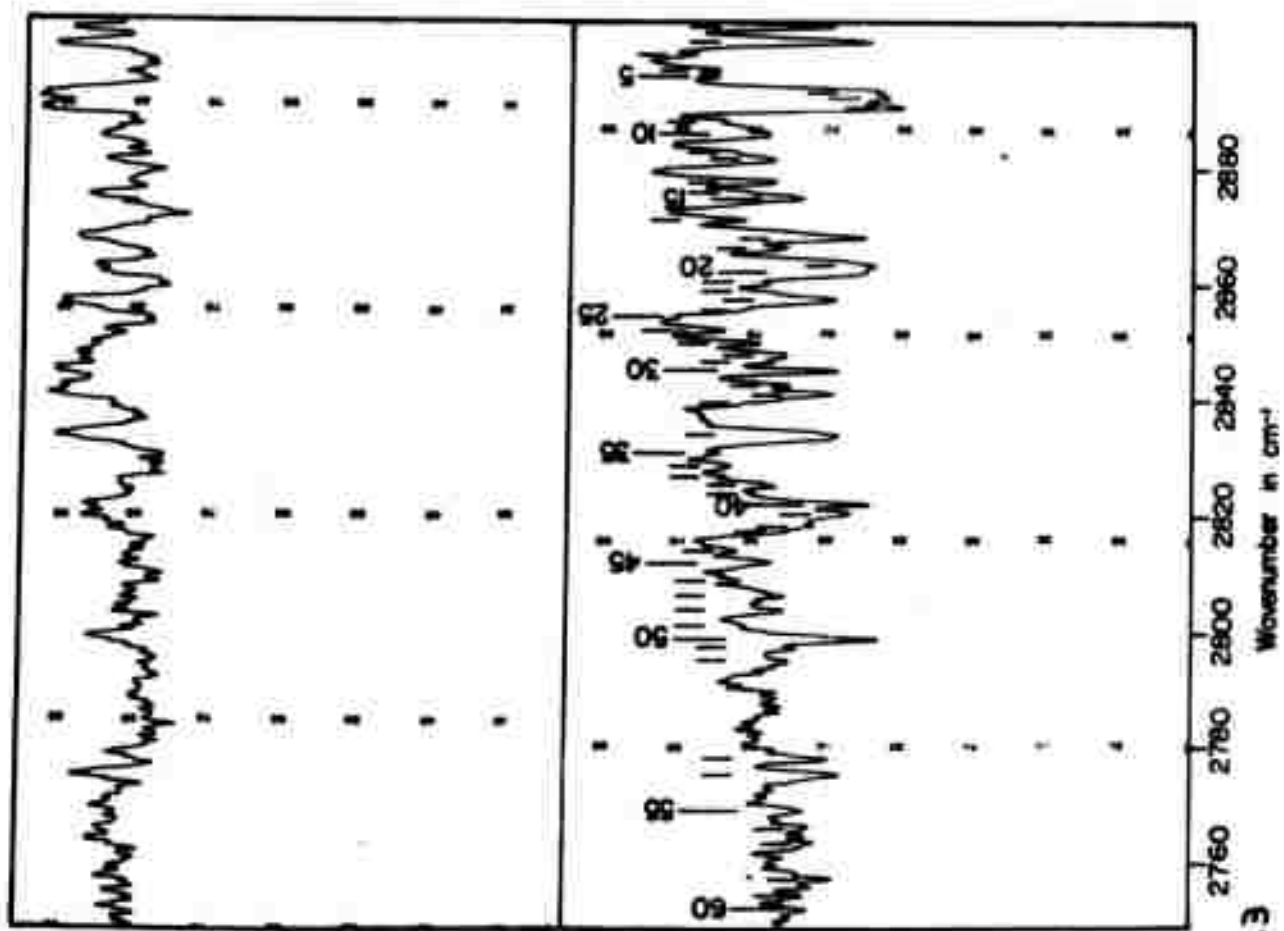


Fig 3

FIG. 4. Absorption and emission spectrum from  $2480\text{ cm}^{-1}$  to  $2380\text{ cm}^{-1}$   
( $4.03\mu$ - $4.20\mu$ ) of an  $11\text{-}1/4$  ft. path of steam at  $600^{\circ}\text{C}$  and  
one atmosphere pressure.

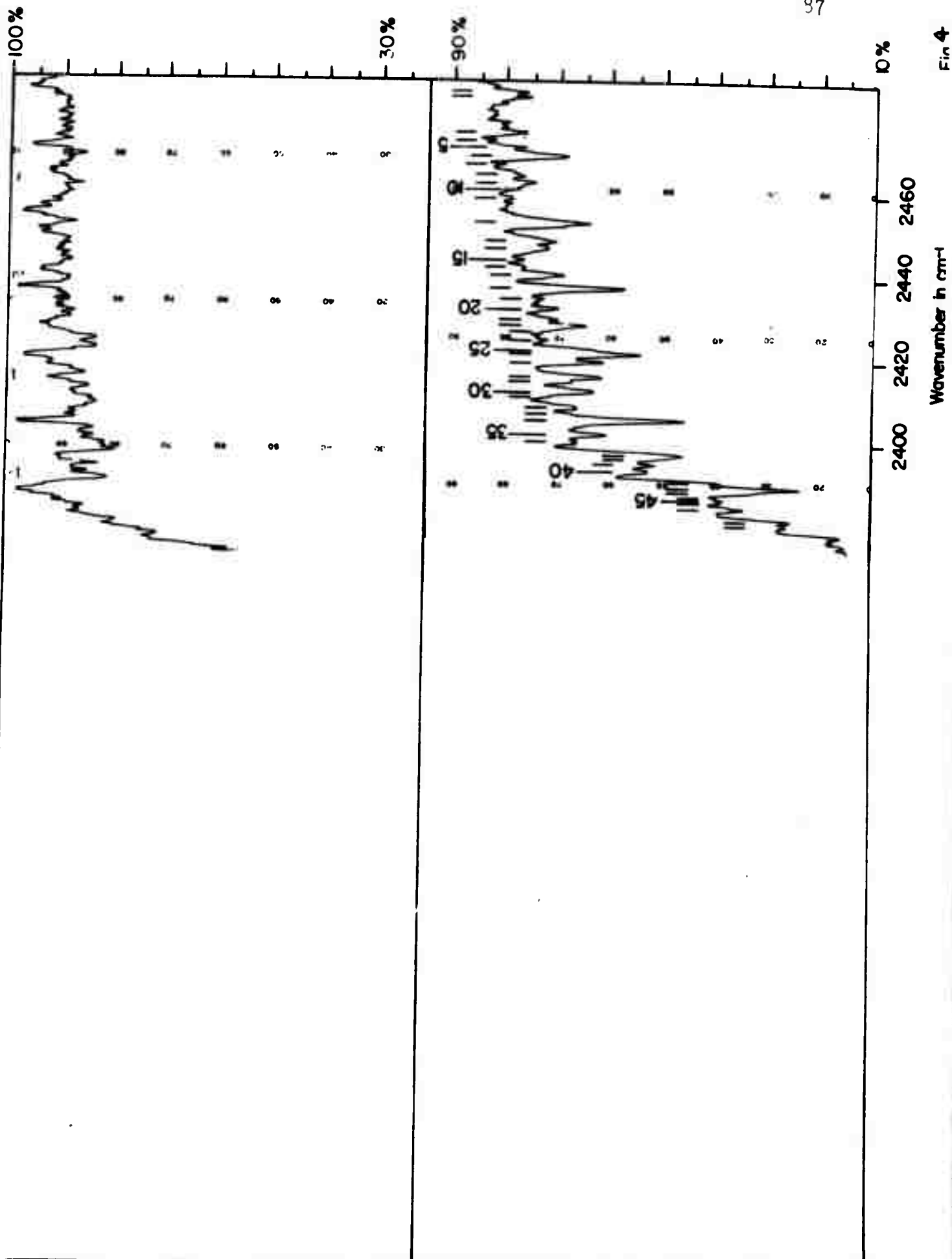


Fig. 4

Fig. 5. Absorption and emission spectrum from  $2300\text{ cm}^{-1}$  to  $1975\text{ cm}^{-1}$  ( $4.35\mu$ - $5.06\mu$ ) of an 11-1/4 ft. path of steam at  $600^{\circ}\text{C}$  and one atmosphere pressure.

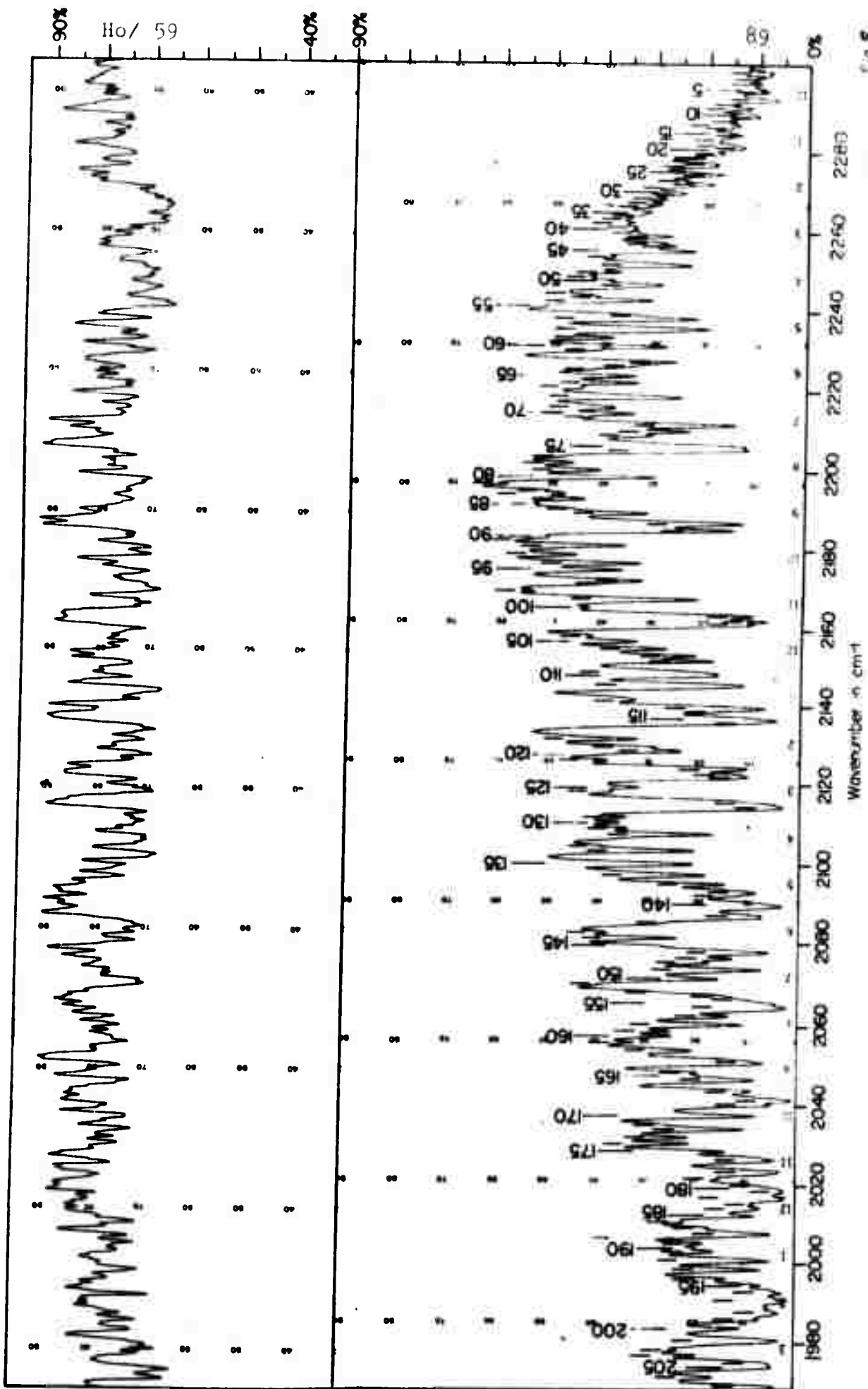


Fig. 5

Fig. 6. Absorption spectrum from  $1260\text{ cm}^{-1}$  to  $1170\text{ cm}^{-1}$  ( $7.91\mu$ - $8.62\mu$ ) of an  $11\text{-}1/4$  ft. path of laboratory air at  $600^{\circ}\text{C}$  and one atmosphere pressure. Humidity was 79% at  $82^{\circ}\text{F}$ . The following lines: Nos. 4, 5, 6, 21, 28, 29, 33, 56, 58, 65, 77, 78, 88, 92, 105, and 119 are in the local high absorption areas. To avoid total absorptions around these lines, the whole spectral range was investigated under hot air condition.

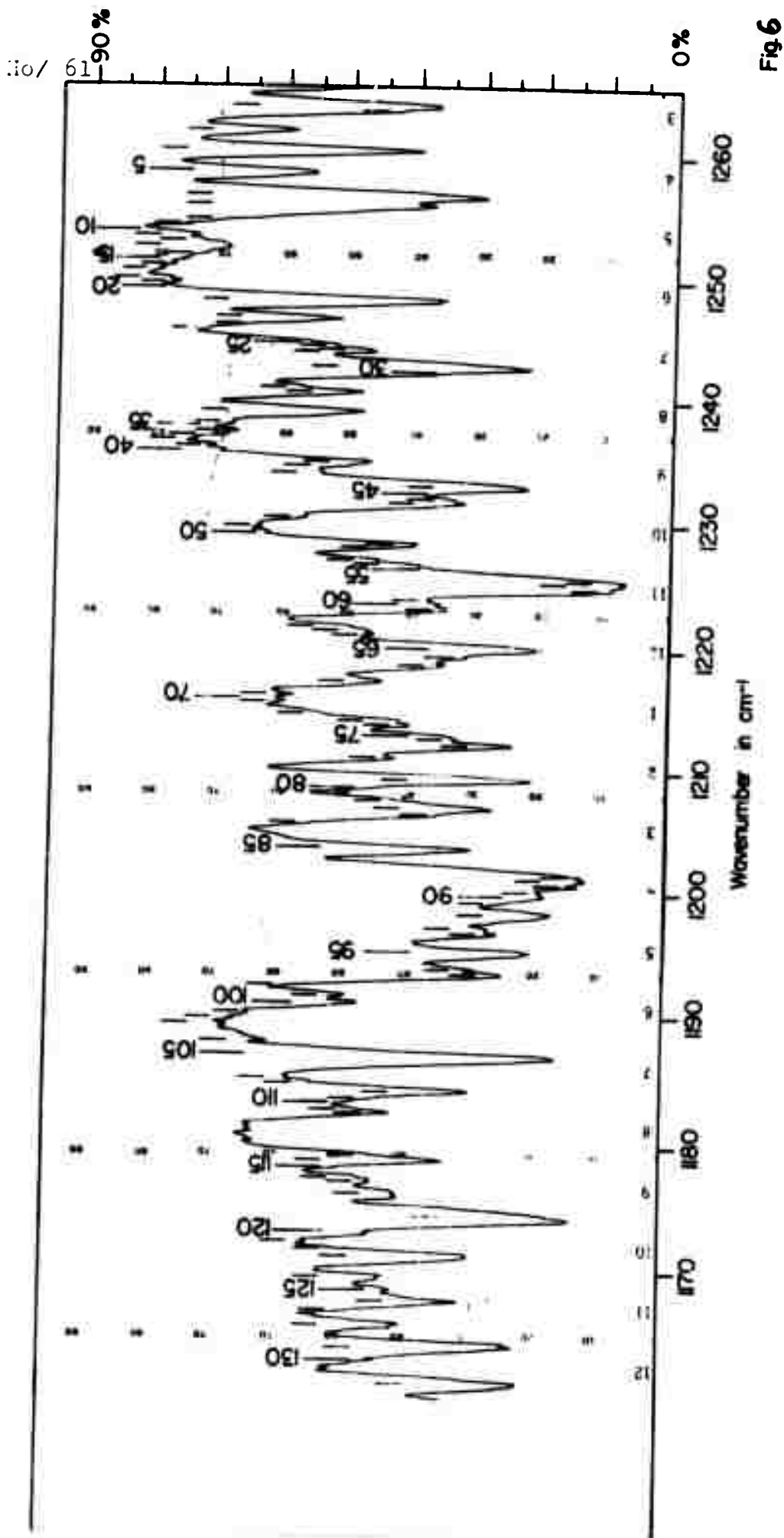


Fig. 7. Absorption and emission spectrum from  $1179\text{ cm}^{-1}$  to  $1060\text{ cm}^{-1}$  ( $8.62\mu\text{-}9.43\mu$ ) of an 11-1/4 ft. path of steam at  $600^{\circ}\text{C}$  and one atmosphere pressure.

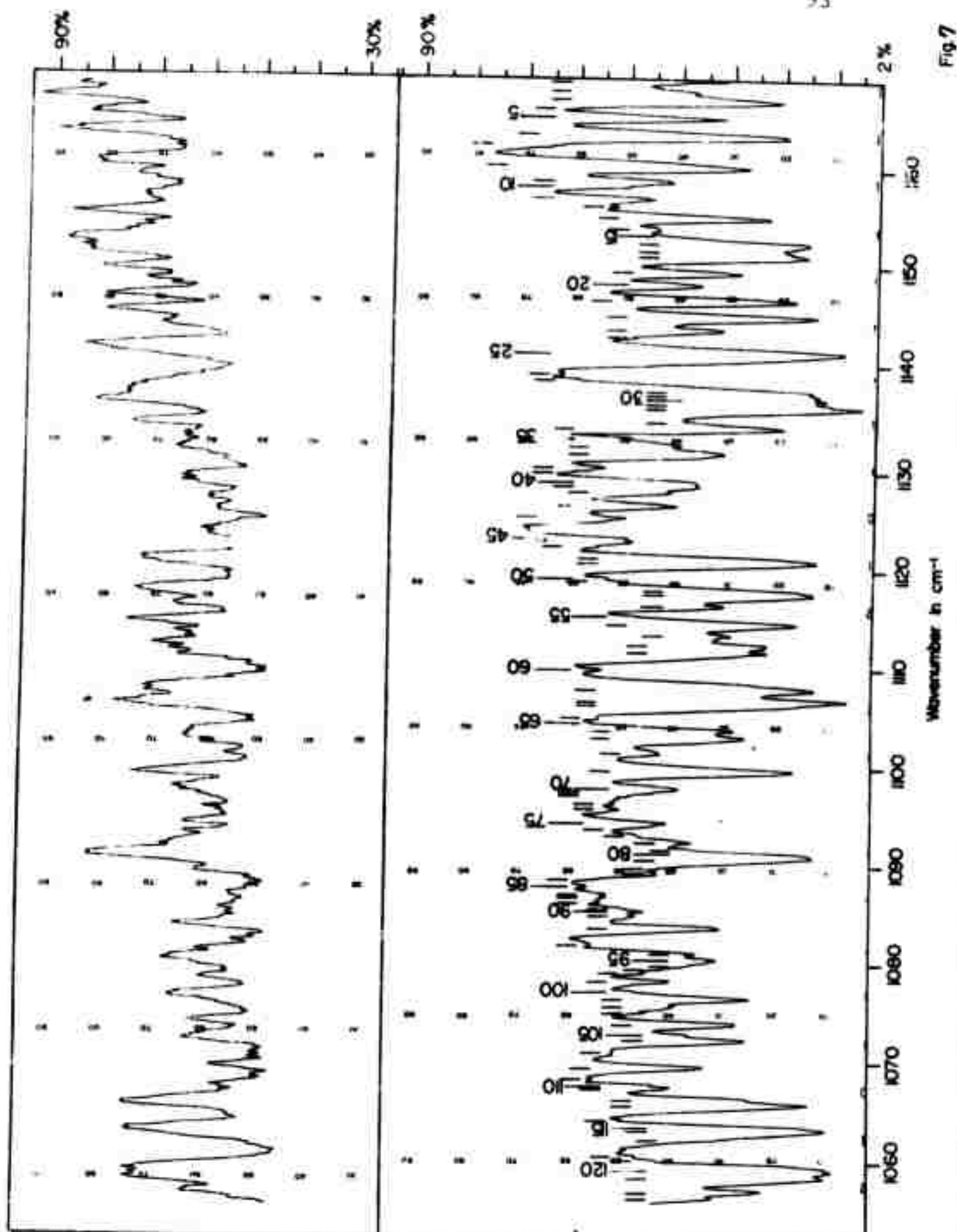


Fig. 7

Fig. 3. Absorption and emission spectrum from  $1060\text{ cm}^{-1}$  to  $940\text{ cm}^{-1}$  ( $9.43\mu$ - $10.63\mu$ ) of an  $11\text{-}1/4\text{ ft.}$  path of steam at  $600^{\circ}\text{C}$  and one atmosphere pressure.

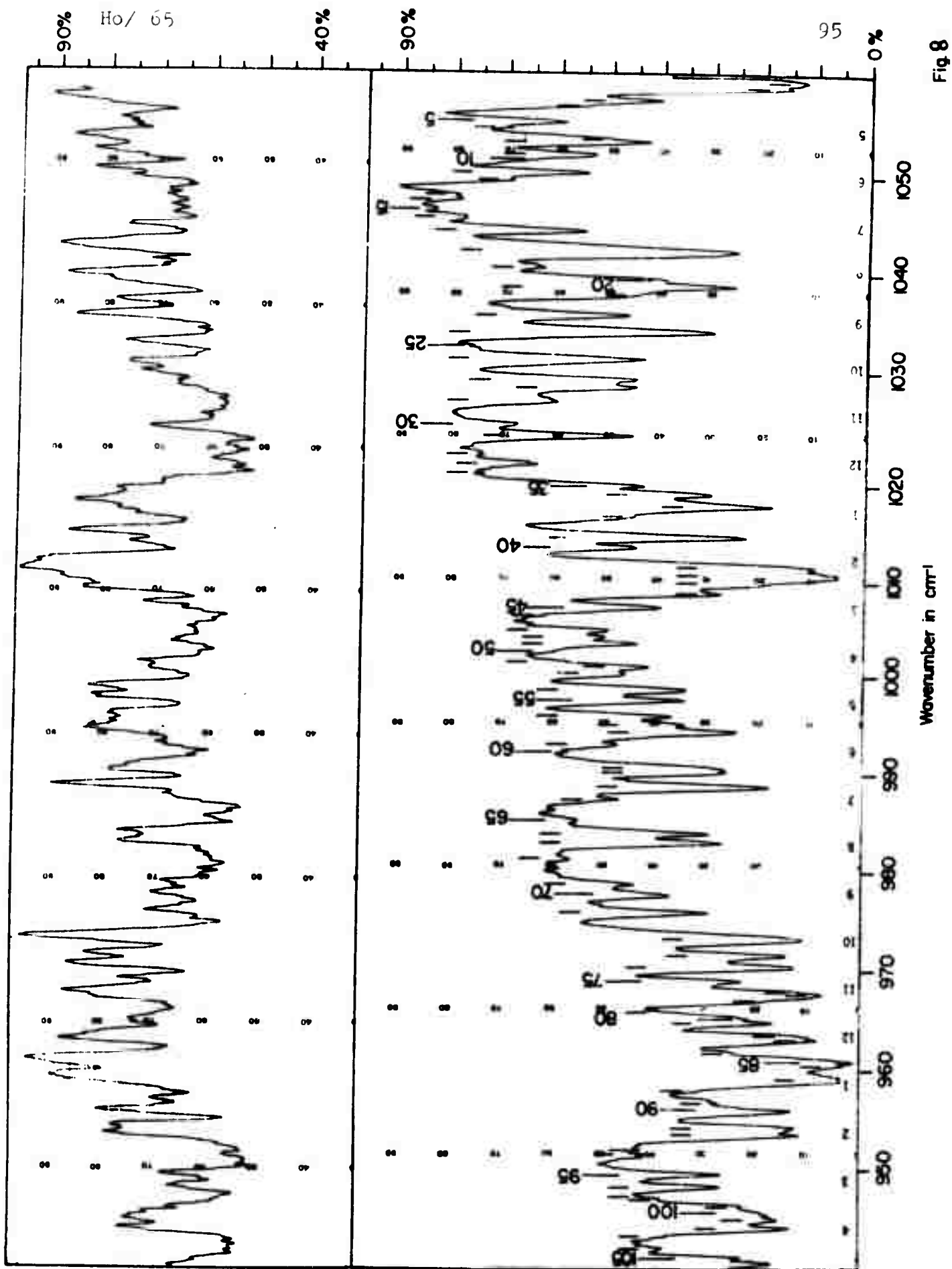


Fig. 9. Absorption and emission spectrum from  $940\text{ cm}^{-1}$  to  $820\text{ cm}^{-1}$  ( $10.63\mu$ - $12.20\mu$ ) of an 11-1/4 ft. path of steam at  $600^{\circ}\text{C}$  and one atmosphere pressure.

Fig 9

Wavenumber in  $\text{cm}^{-1}$

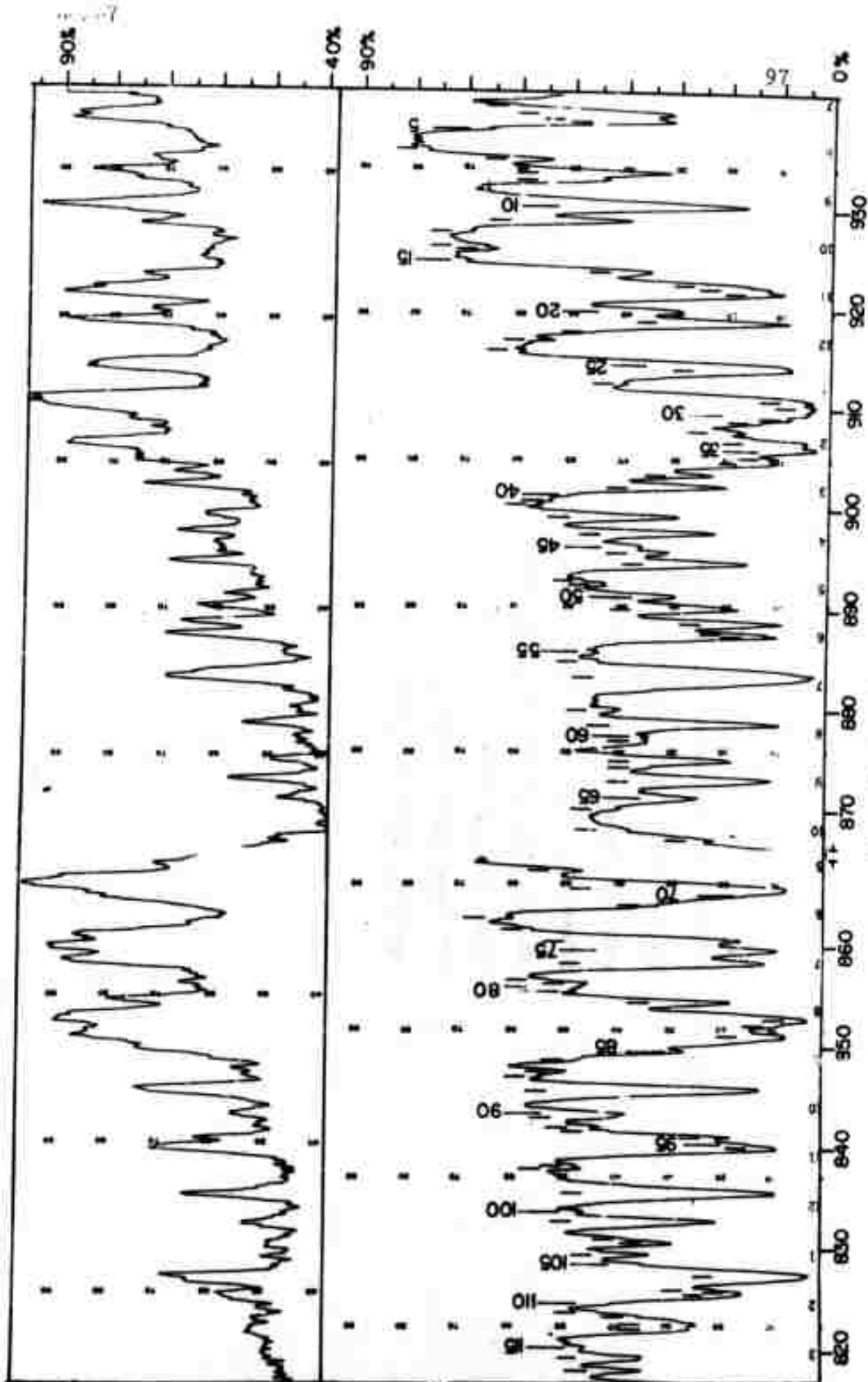


Fig. 10. Absorption and emission spectrum from  $820\text{ cm}^{-1}$  to  $715\text{ cm}^{-1}$  ( $12.20\mu$ - $13.98\mu$ ) of an  $11\text{-}1/4$  ft. path of steam at  $600^{\circ}\text{C}$  and one atmosphere pressure. Line Nos. 5, 13, 18, 25, 28, 39, 49, 50, 56, 73, 75, 76, 78, 85, and 89 are in the local high absorption areas. Steam was shut off temporarily when it was scanning in these spectral areas to avoid total absorptions.

Ho/ 69

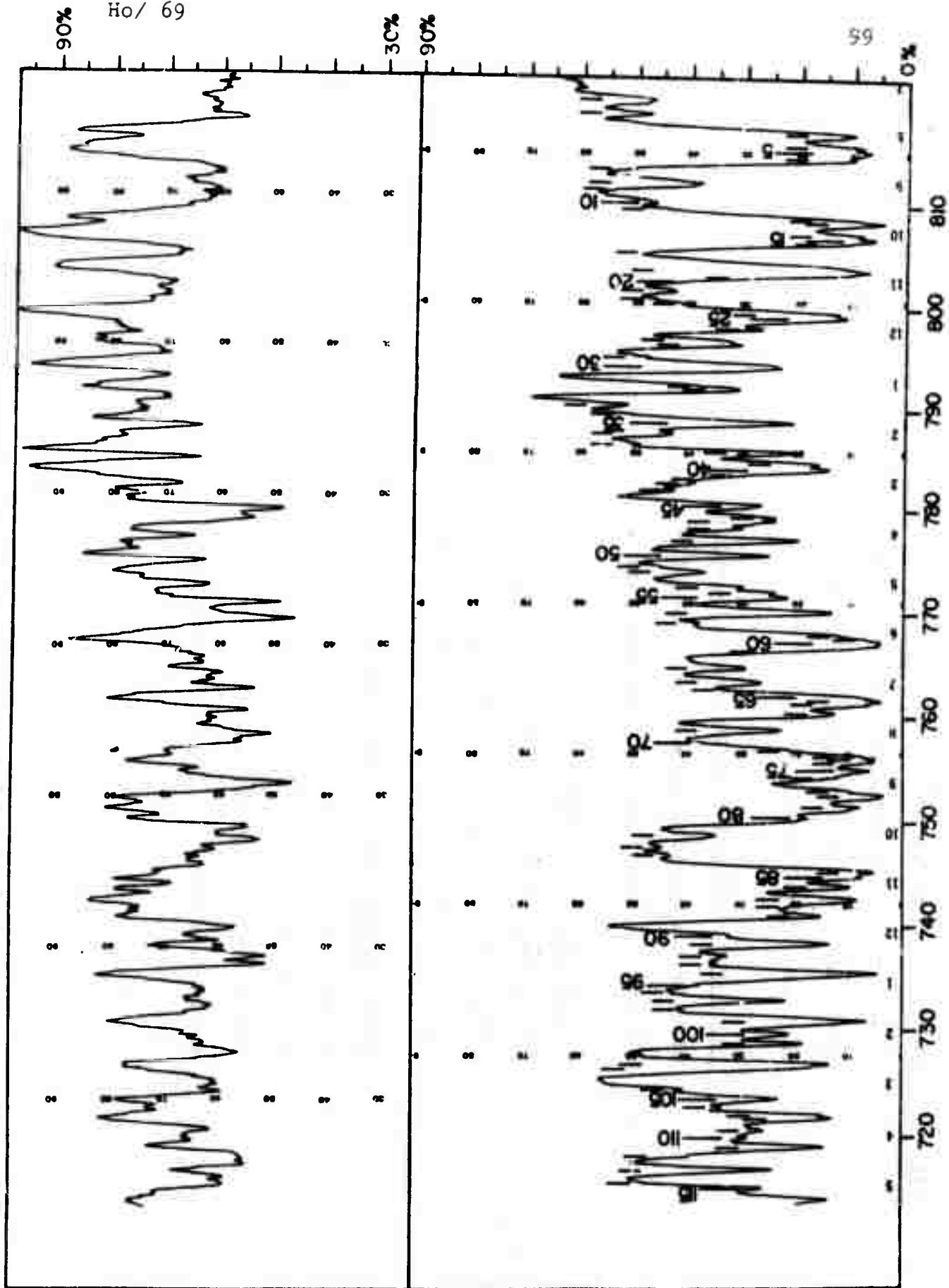


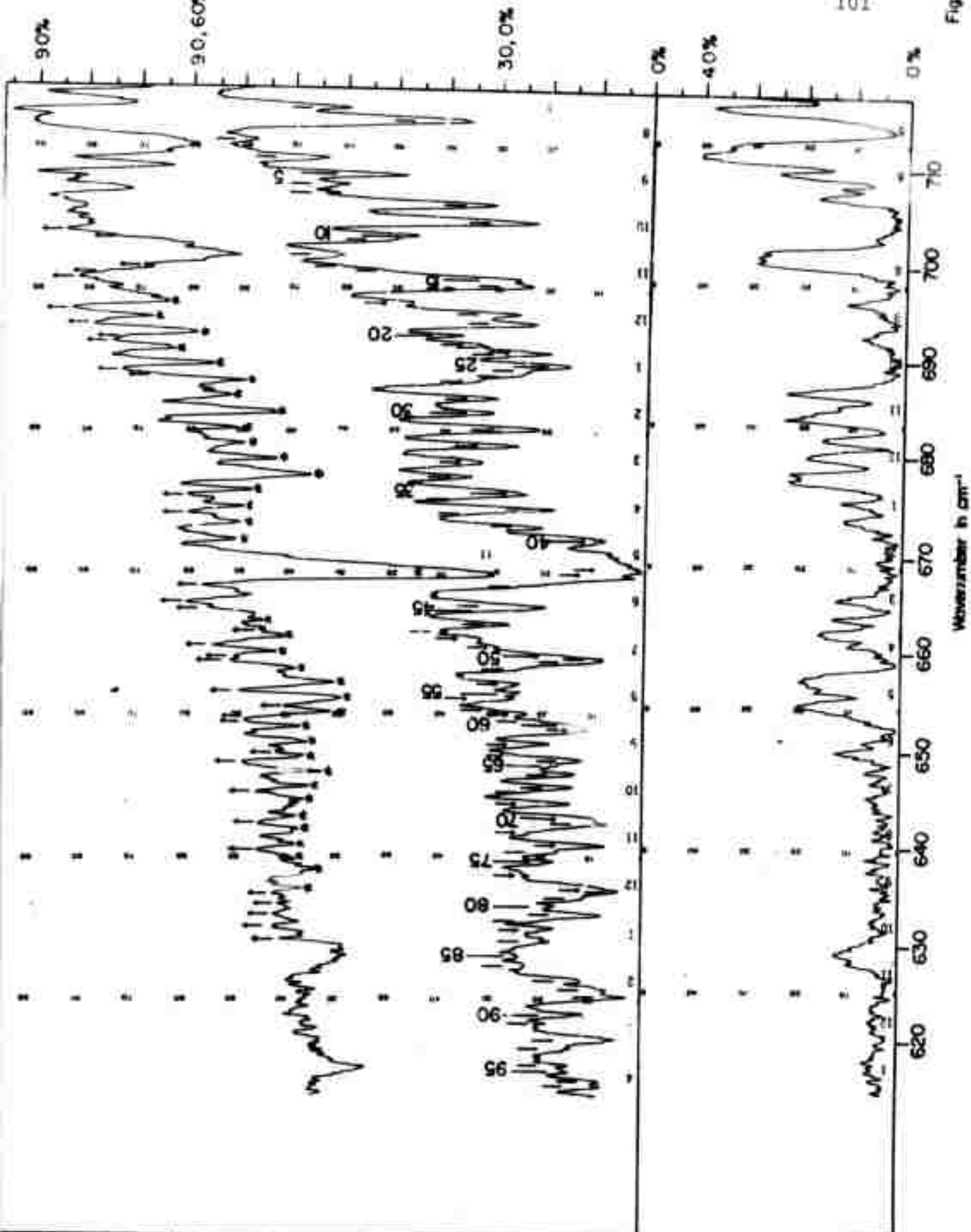
Fig. 10

Fig. 11. Spectrum from  $715\text{ cm}^{-1}$  to  $615\text{ cm}^{-1}$  ( $13.98\mu$ - $16.25\mu$ ), temperature  $600^{\circ}\text{C}$ . Top curve, steam emission spectrum. Middle curve, hot air absorption spectrum. Bottom curve, steam absorption spectrum. Each curve has the same slitwidth---.377 mm.

Top curve: Asterisk lines are believed to be atmospheric carbon dioxide absorptions picked up in the 6.5 foot air path outside the hot cell. Upward arrow lines are pure water vapor emission spectra.

Middle curve: Downward arrows indicate spectral positions of natural atmospheric carbon dioxide. Pure water vapor absorption (lines without arrows) are confirmed by the corresponding emission lines on the top curve. Humidity was 79% at  $82^{\circ}\text{F}$ .

Bottom curve: Water vapor absorptions are high in the whole spectral region. It suggests absorptions between line no. 28 and no. 42 are pure atmospheric carbon dioxide spectra. Spectra following line no. 61 are mainly due to water vapor absorption other than carbon dioxide.



REFERENCES

1. D.J. Lovell, "An Atlas of Air Absorptions in the Infrared," Astronomy Research Facility, University of Massachusetts, Amherst, Mass. (Report #49/243), June, 1969.
2. J.H. Taylor, W.S. Benedict, John Strong, "Infrared Spectra of  $H_2O$  and  $CO_2$  at  $500^\circ C$ ," Johns Hopkins University, Baltimore, Maryland [Contract Nonr 248(01)], March 1, 1952.
3. W.S. Benedict, H.H. Claassen, and J.H. Shaw, "Absorption Spectrum of Water Vapor Between 4.5 and 13 Microns," Journal of Research of the National Bureau of Standards 49, No. 2, (August, 1952).
4. J.R. Izatt, "Self and Foreign Gas Broadening in the Pure Rotation Spectrum of Water Vapor, 475 to 690 Wavenumber," Laboratory of Astrophysics and Physical Meteorology, Johns Hopkins University, [Contract Nonr 248(01)], 1960.
5. R. Goldstein, "Measurements of Infrared Absorption by Water Vapor at Temperatures to  $1000^\circ K$ ," J. Quan. Spectrosc. Radiat. Transf. 4, No. 2, 343-352 (March/April, 1964).
6. Y.B. Aryeh, "Line Width and Intensities in the Wings of the  $\nu_2$  Water Vapor Band at  $400^\circ K$  and  $450^\circ K$ ,"

- J. Quan. Spectrosc. Radiat. Transf. 7, No. 1, 211-214 (Jan./Feb., 1967).
7. C.C. Ferriso, and C.B. Ludwig, "Spectral Emissivities and Integrated Intensities of the 1.87-, 1.38-, 1.14 $\mu$  H<sub>2</sub>O Bands Between 1000 and 2200°K," J. Chem. Phys. 41, No. 6, 1668-1674 (June, 1964).
  8. W.S. Benedict, A.M. Bass, and E.K. Plyler, "Flame-Emission Spectrum of Water Vapor in the 1.9 Micron Region," J. Research Nat'l Bureau Stand. 49, No. 2, 91-132 (Feb., 1959).
  9. J. Auman, Jr., "The Infrared Opacity of Hot Water Vapor," The Astrophysical Journal 148, No. 1, Part 1, 313 (April, 1967).
  10. P. Varanasi, S. Chou, and S.S. Penner, "Absorption Coefficients for Water Vapor in the 600-1000 cm<sup>-1</sup> Region," J. Quant. Spectrosc. Radiat. Transfer 8, 1537-1541 (August, 1968).
  11. David M. Gates, Robert F. Calfee, David W. Hansen, and W.S. Benedict, "Line Parameters and Computed Spectra for Water Vapor Bands at 2.7 $\mu$ ," National Bureau of Standard Monograph 71, (issued August 3, 1964).
  12. W.S. Benedict, Robert F. Calfee, "Line Parameters for the 1.9 and 6.3 Micron Water Vapor Bands," ESSA Professional Paper 2, U.S. Department of Commerce, Washington, D.C., (June, 1967).

13. International Union of Pure and Applied Chemistry  
Commission on Molecular Structure and Spectroscopy,  
Tables of Wavenumbers for the Calibration of  
Infrared Spectrometers, (Butterworths, Washington,  
1961).  
HCl,  $3059.32\text{ cm}^{-1}$ -- $2650.22\text{ cm}^{-1}$ , pp. 572-573  
HBr,  $2749.12\text{ cm}^{-1}$ -- $2372.29\text{ cm}^{-1}$ , pp. 574-575  
CO,  $2241.68\text{ cm}^{-1}$ --- $2013.35\text{ cm}^{-1}$ , pp. 580-581  
NH<sub>3</sub>,  $1212.68\text{ cm}^{-1}$ -- $753.61\text{ cm}^{-1}$ , pp. 588-589  
CO<sub>2</sub>,  $701.69\text{ cm}^{-1}$ --- $629.46\text{ cm}^{-1}$ , pp. 592-593
14. S.Y. Ho, "Long-Path Infrared Spectra of CO, NO<sub>2</sub>,  
NO, SO<sub>2</sub>, and N<sub>2</sub>O Observed in a Simulated Atmosphere  
in Trace Amounts," Astronomy Research Facility,  
University of Massachusetts, (NR No. 015-301).
15. R.M. Goody, "Atmospheric Radiation, 1. Theoretical  
Basis," Oxford University Press, p. 180, (1964).
16. E.F. Barker and W.W. Sleator, "The Infrared Spectrum  
of Heavy Water," J. Chem. Phys. 3, 660 (1935).
17. W.S. Benedict, N. Garlar, and E.K. Plyler, "The  
Vibration-Rotation Spectrum of HDO," J. Chem.  
Phys. 21, No. 7, 1302-1303 (July, 1953).
18. D. J. Iovell and J. D. Strong, "Long-Path Study of In-  
frared Absorption and Emission", Appl. Opt. 8, 1673  
(Aug. 1969).
19. J. Strong, "Procedures for Infrared Spectroscopy", Appl.  
Opt. 11, 2331 (Oct. 1972).

## ATTACHMENT D

HIGH RESOLUTION INFRARED SPECTROMETER  
WITH MULTIPLEX ADVANTAGE

Peter Hansen

John Strong

Astronomy Research Facility  
Department of Physics and Astronomy  
University of Massachusetts  
Amherst, Massachusetts 01002

August, 1972

ABSTRACT

A high resolution ( $0.07 \text{ cm}^{-1}$ ) infrared spectrometer for the wavelength range of 5 to  $25\mu$  is described. The instrument employs an echelle grating and alkaline halide lenses instead of mirrors. A helium-cooled ( $1.9^\circ\text{K}$ ) germanium bolometer is used as a detector. In spectral regions where non signal-dependent noise predominates, a multiplex mask (instead of a single slit), generated from cyclic Hadamard matrices, is introduced at the exit focal plane. The signal is then chopped and de-dispersed by another pass through the spectrometer and focused on the single detector. The multiplexing results in a theoretical S/N gain of 5.6. Matrix

inversion is done by digital computer. Sample absorption spectra are shown as well as comparisons of single slit and multiplex slit scans.

### S/N Gain in Multiplex Spectrometers

Multiplexing as it applies to spectrometry refers to the process of simultaneously observing many spectral frequencies thus gaining a signal to noise (S/N) advantage for non signal-dependent noise, i.e. random noise. This technique is used to good advantage in the infrared, where many systems are detector noise limited. It is most widely applied in Fourier transform spectroscopy (FTS), where a Fourier transformation of the output of a two beam interferometer yields the desired spectrum. However, recently multiplexing has been successfully accomplished using arrays of open and opaque slits (corresponding to the elements in cyclic Hadamard matrices) placed at the exit focal plane of a conventional dispersive spectrometer. This procedure is referred to as Hadamard transform spectroscopy (HTS). Such a system is described here.

Fig. 1 schematically compares the two major multiplexing techniques with a conventional monochromator and Fig. 2 indicates the advantages gained by the use of FTS and HTS.

### The Instrument

Fig. 3 illustrates the basic spectrometer. Radiation passes through the entrance slit which is located at the focus of a 16 cm NaCl-KBr lens.<sup>1</sup> After passing through the lens, the radiation is dispersed by the echelle grating and reflected back through the lens. The spectrum obtained is focused on the entrance slit. A 45-degree reflecting surface (Fig. 4) just in front of the entrance slit reflects the spectrum falling on either side of the entrance slit cutout (Fig. 4). Either a single slit or the multiplex slits are placed at the downward focus--the exit focal plane. After passing through the slit, or slits, the spectrum is again reflected by the mirror  $m_2$  (Fig. 4) and is returned to the lens. This reflection is at slightly less than 90 degrees so that the chief ray crosses the optic axis when it reaches the lens. Since the image is inverted by the two reflections, the spectrum is now de-dispersed<sup>2</sup> by the grating. In multiplex mode of operation, the final images of the multiplex slits are superimposed. They fall at a distance above the optic axis, at a focal plane approximately at the entrance slit focal plane. The mirror  $m_3$  located 5 cm in front of this focal plane puts the de-dispersed spectrum on a 3:1 image slicer.<sup>1</sup> The entrance and exit slits are 0.38 mm wide and 12 mm long. The image slicer transforms the rectangular

exit area from 0.38 x 12 mm to a circumscription rectangle of 1.2 x 4 mm dimensions. And the diverging spectrum ( $f/16$ ) is focused onto the 1/2 x 1 mm detector chip at 4-fold reduction by a 2.5 cm NaCl-KBr achromat ( $f/4$ ).<sup>1</sup> The Airy diffraction disks of the achromatic lenses at  $\lambda \approx 6\mu$  are less than half the slit width (0.38 mm).

The echelle grating, due to its controlled groove shape and high angle of incidence, directs substantially all of the incident energy into one or two of the higher orders. The grating has a ruled area of 206 x 102 mm, a blaze angle of  $63.26^\circ$  and is ruled at 31.64 lines/mm. As an example, in the  $6\mu$  region, it is normally operated in the 9th order where the angle of incidence (and reflection) is close to the blaze angle. The projected grating area near the blaze angle is 10 x 10 cm which matches the stopped down area of the large NaCl-KBr lens. The theoretical resolving power is equal to the number of wavelengths contained in the path difference of the grooves at the outer edges of the grating. This is  $\Delta\nu = \frac{1}{2D} = \frac{1}{37 \text{ cm}} = .027 \text{ cm}^{-1}$  for our grating. A resolving power of  $.07 \text{ cm}^{-1}$  is achieved in practice.

Square wave chopping of the radiation is accomplished with a three-blade rotary chopper turning at 2000 rpm. This results in a satisfactory chopping frequency for the detector (100 Hz). The chopper is machined from a 38 cm

diameter aluminum disk, and it is driven by a synchronous motor. Since an area of  $1.2 \times 4.8$  cm (multiplex mask dimensions) is chopped, a large chopper diameter is necessary to assure that the spectral elements at the outer edges of the multiplex mask are chopped nearly in phase with those in the center, and that the edge of the chopper blade spends nearly equal time traversing each spectral element. The chopper also provides a reference signal to a lock-in amplifier; and, since the amplifier makes use of only the 1st harmonic of the chopped signal, square wave modulation is desirable as the peak amplitude of the first harmonic exceeds the amplitude of the square wave by a factor of  $4/\pi$ . Also, chopping the second pass<sup>3</sup> instead of the first, assures that unwanted scattered radiations reaching the detector are not detected, e.g. reflections of much more intense first pass from the surfaces of the 6" lens.

The detector is a liquid helium cooled doped germanium bolometer (Infrared Laboratories, Tucson, Arizona). Pumping on the helium reduces the operating temperature to  $1.9^\circ\text{K}$ . At this temperature the noise equivalent power (NEP) has been measured and calculated to be less than  $1 \times 10^{-13} \text{ W/Hz}^{1/2}$ . A cold ( $1.9^\circ\text{K}$ ) band-pass filter is placed in front of the detector chip to suppress unwanted signals.

For random noise, the signal-to-noise ratio increases with the square root of the observation time. A 253 element multiplex mask is employed in our spectrometer (Fig. 5). 127 elements are exposed to the spectrum at all times. Since half of the elements represent opaque slits, the multiplex slits increase the integrated observation time by a factor of 64; and, after matrix inversion, the signal-to-noise ratio is increased by a factor of  $\sqrt{5.6}$ , as compared to an equivalent single slit scan using equal total observation time.

The multiplex mask is stepped 126 times during a measurement and its transparent and opaque slits generate a 127 square cyclic<sup>4</sup> Hadamard matrix having zeros (transparent) and ones (opaque) as elements. This is a suitable form for digital computation. If

$$[H^{127}] [S] = [I]$$

where  $[H^{127}]$  is the square Hadamard matrix generated by the multiplex slits,  $[S]$  is the one-dimensional matrix containing the 127 unknown spectral elements, and  $[I]$  is the one-dimensional matrix containing the 127 observed intensities; then

$$[S] = [H^{127}]^{-1} [I]$$

This equation is solved by computer. To minimize computing time, the  $[H^{127}]$  matrix is inverted only once and then stored, thus allowing use of computing facilities having

less than 8K memories. The present computer program provides for both a numerical listing of the multiplex spectrum and for a graphical plot. Total computing time is 3 seconds and the spectrum plot is completed within 7 minutes.

In spectral regions where source and/or background noise predominate, a single slit is used. Under these conditions the multiplex advantage does not come into play. The optical path for single and multiplex spectra is identical and single slit spectra may be obtained by either stepping the slit or grating rotation.

#### Performance and Measurements

The six micron water vapor bands were chosen for the initial alignment, calibration and performance checks. The echelle grating was used in its ninth order with some overlapping of the eighth order. A cold filter used with the detector passed a wavelength band  $1.25\mu$  wide ( $5.85\mu - 7.1\mu$ ). Wavelength calibration was accomplished by proper identification of water vapor absorption lines.<sup>5,6</sup> The spectrometer was purged with dry air to eliminate all lines in its path length. A globar was the source and all the measurements were made at low pressures in a 92 meter path length absorption cell. Fig. 6 illustrates a typical water vapor spectrum obtained with a single slit. The 16 cm KBr-NaCl collimator-telescope lens was

bolometrically focused on the slits for maximum signal and highest resolution.

The cold bandpass filter was changed ( $12.1 - 15.4\mu$ ) and the LIF detector window was replaced with NaCl to observe performance at longer wavelengths. The focus of the alkaline halide lenses remained the same at  $14\mu$  as at  $6\mu$ , an indication of their good achromatism in the infrared. Fig. 7 illustrates the resolution obtained in the  $6\mu$  and  $14\mu$  regions.

The multiplex advantage is best realized at very low signal levels. A stepped single slit scan was made at the exit focal plane with the grating in a fixed position and the slits set at 0.38 mm, the spectrometer purged with dry air, and with very little energy incident on the entrance slit. The slit was then replaced with the multiplex slits and another spectrum was obtained. The total observation time was the same for both single slit and multiplex measurements. The two results are shown in Fig. 8. The single slit spectrum is simply the detector output. The multiplex spectrum is obtained by connecting the 127 consecutive computer output points by straight lines. It is apparent that the signal-to-noise ratio is significantly improved in the multiplex spectrum. The strong "absorption line" in the center is caused by the entrance slit cutout. Its equivalent spectral width is less than  $0.2 \text{ cm}^{-1}$ . The entrance slit cutout is also an

example of a property of HTS mentioned earlier (Fig. 2): wavelength filtering. At  $700\text{ cm}^{-1}$  ( $14.3\mu$ ) a multiplex spectrum covers six wavenumbers--the position of the grating determines the spectral location of this frequency interval.

We presently have bandpass filters covering the range from  $5.8\mu$  to  $25\mu$  and two sets of alkaline halide achromats are used to cover this region: KBr-NaCl for the  $5.8$  to  $15\mu$  region, and KBr-KI for the  $15$  to  $25\mu$  region. The overlapping order problem at short wavelengths can be overcome with a more densely ruled echelle grating, e.g., 70 lines per millimeter. The spectrometer is being interfaced with several absorption cells of various absorption path lengths.

#### Acknowledgments

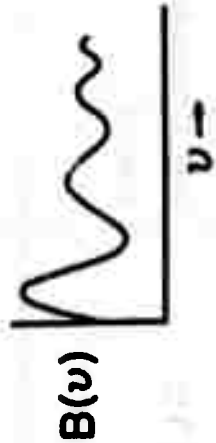
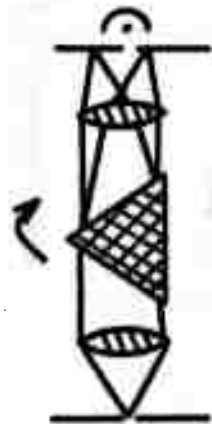
The construction and assembly of the spectrometer was supported by ARPA under Contract No. F19628-70-C-0296; the detector and grating were provided by ESSA under Contract No. E-174-69(N). Sprague Electric Company photo-etched the multiplex slits.

Figure Captions

- Fig. 1      Schematic representation of conventional monochromator and the two major multiplexing methods.
- Fig. 2      Comparison of the two multiplexing systems indicating advantages over conventional spectroscopy.
- Fig. 3      (a) Basic HTS spectrometer, and (b) equivalent optical path.
- Fig. 4      View of exit focal plane with multiplex slits, corner reflector and chopper.
- Fig. 5      253 slot multiplex mask
- Fig. 6      Water vapor absorption at three pressures over 92 meter path length.
- Fig. 7      High resolution spectra. (a) Water vapor at  $P = 0.300$  mm, 92m path length. (b) carbon dioxide at  $P = 20$ mm, 2.2m path length.
- Fig. 8      Comparison of single slit and multiplex scans.

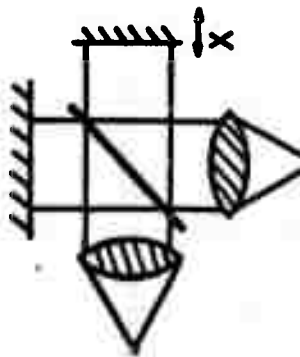
# CONVENTIONAL

$$(S/N=1)$$

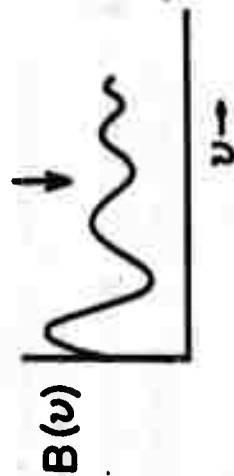


# FOURIER

$$(S/N=\sqrt{N/2})$$

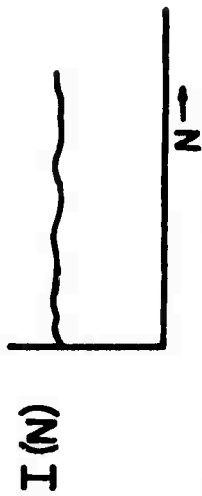
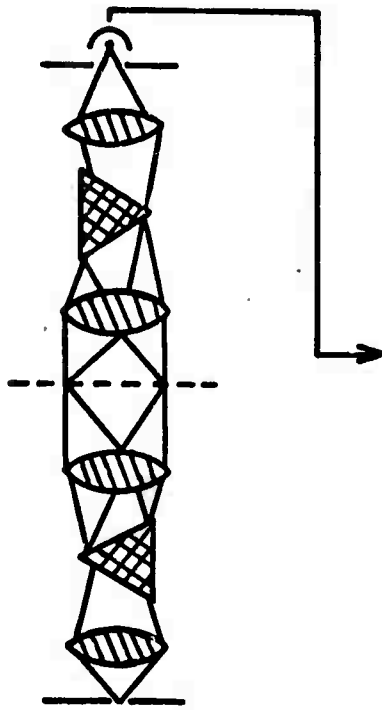


$$\int_{-\infty}^{\infty} I(x) e^{-2\pi i x v} dx$$



# HADAMARD

$$(S/N = N+1/2N^{1/2})$$



$$[S] = [H^N]^{-1} [I]$$

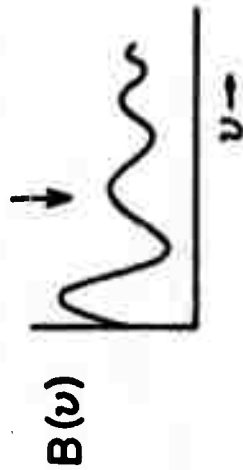


Fig. 1 Schematic representation of conventional monochromator and the two major multiplexing methods.

## COMPARISON OF FTS AND HTS

	SPECTRUM COMPUTATION	INSTRUMENTAL DYNAMIC RANGE	MECHANICAL TOLERANCES	WAVELENGTH FILTERING	THROUGHPUT ADVANTAGE	MULTIPLEX ADVANTAGE
FTS	Most difficult Digital computer a must	Always greater than 50% of maximum signal	Interferometric $\Delta d \approx 10^{-8}$ cm	No	Yes	$\sqrt{N/2}$
HTS	Less difficult Digital computer a must	No inherent dynamic range problem	Micrometric $\Delta d \approx 4 \times 10^{-2}$ cm	Yes	Only for doubly encoded	$(N+1)/2N^2$
MONO- CHROMATOR	None necessary	Same as HTS	Same as HTS	Yes	No	1

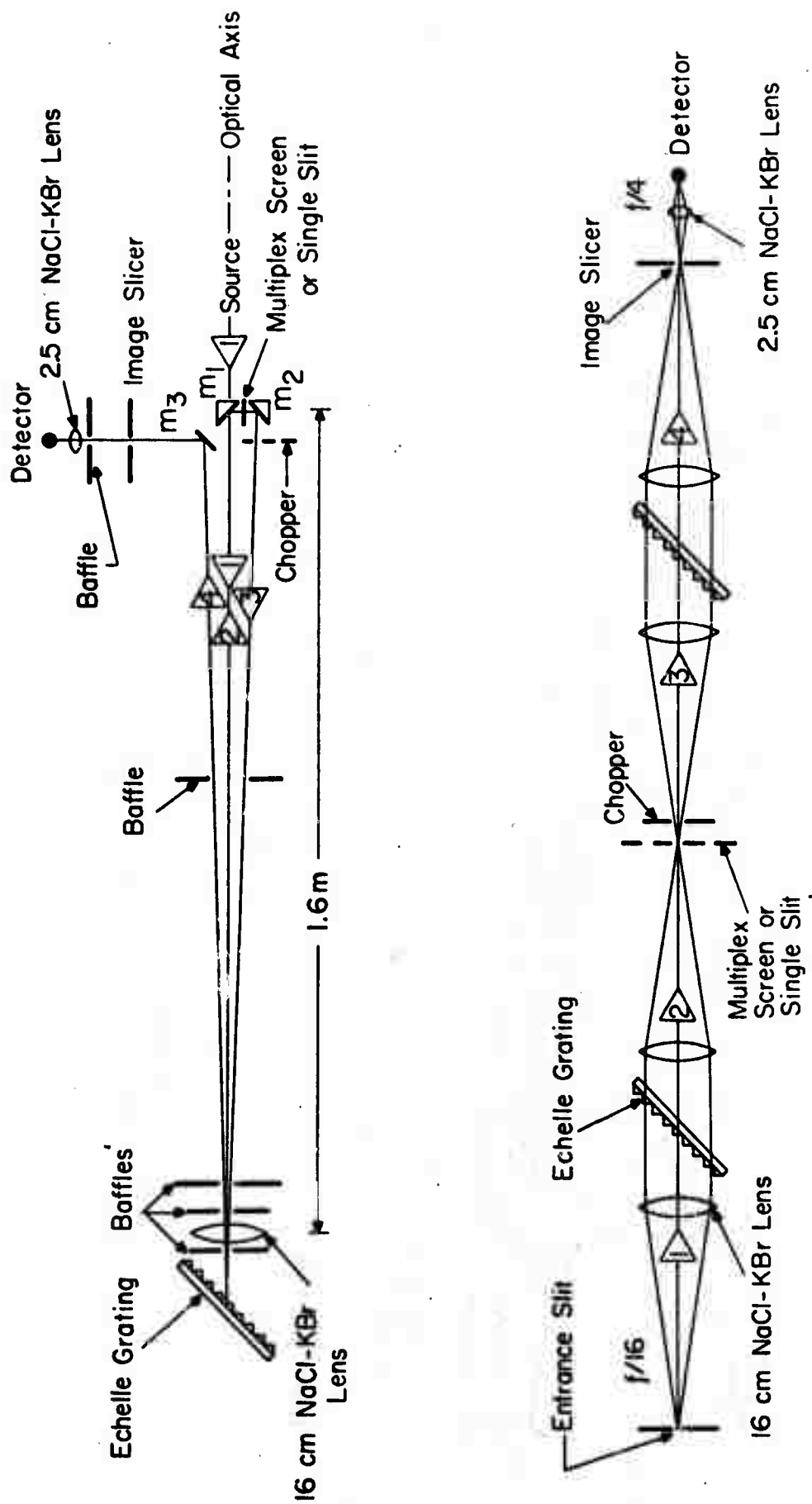


Fig. 3 (a) Basic HTS spectrometer, and (b) equivalent optical path.

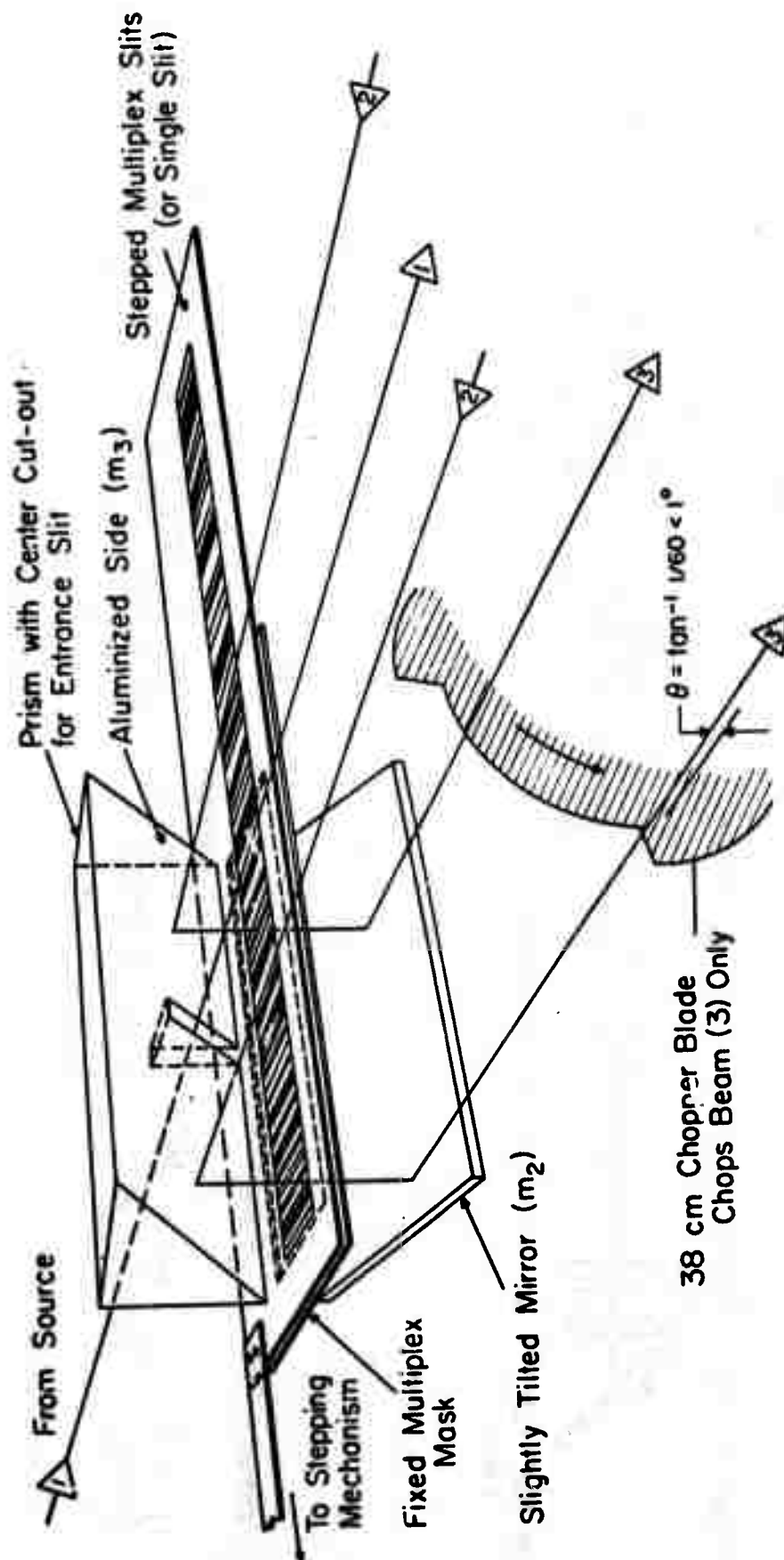




Fig. 5 253 slot multiplex mask.

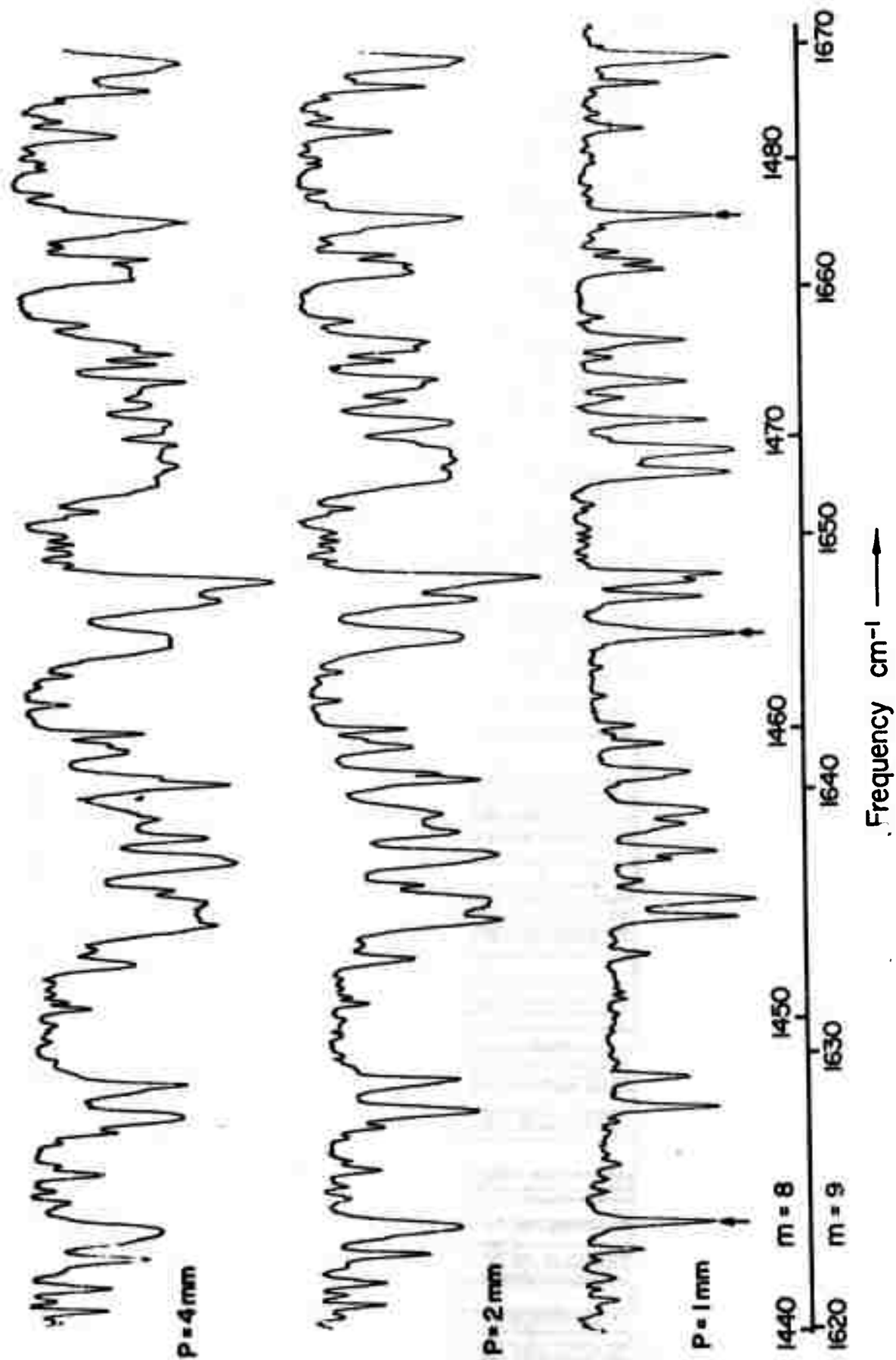
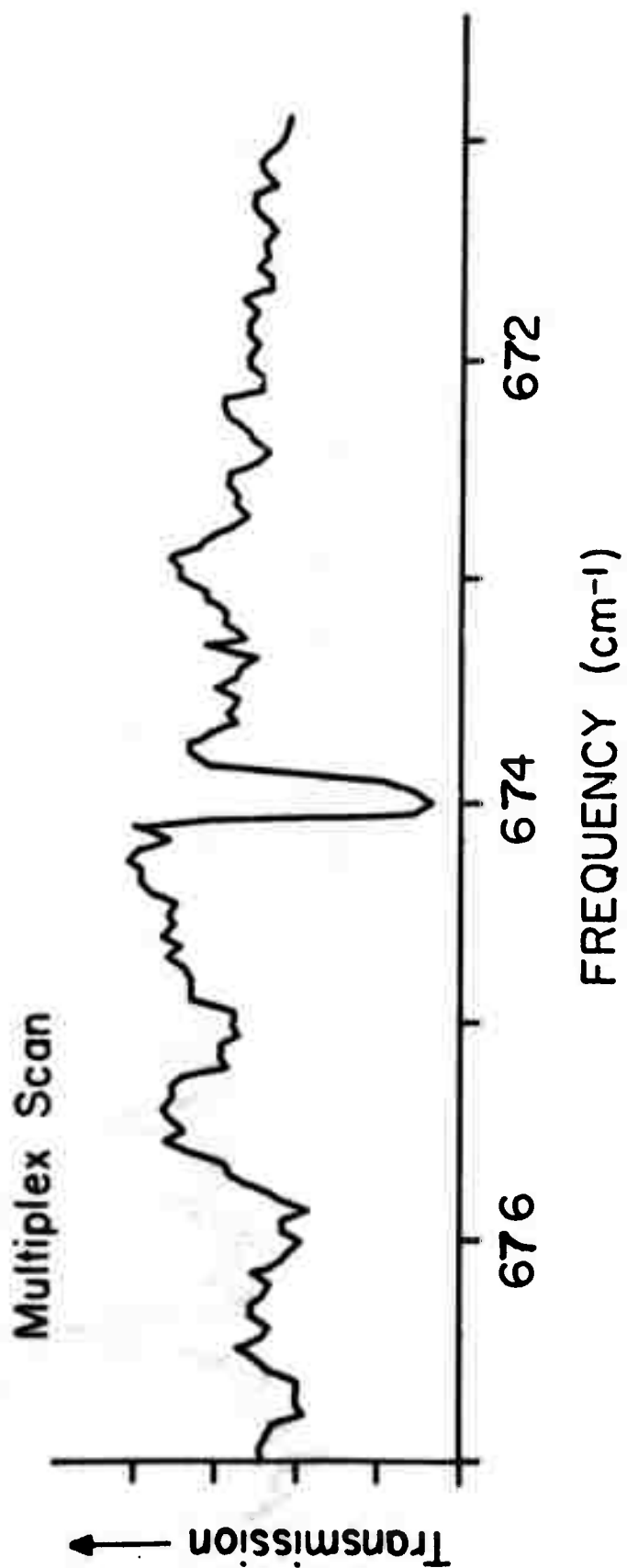
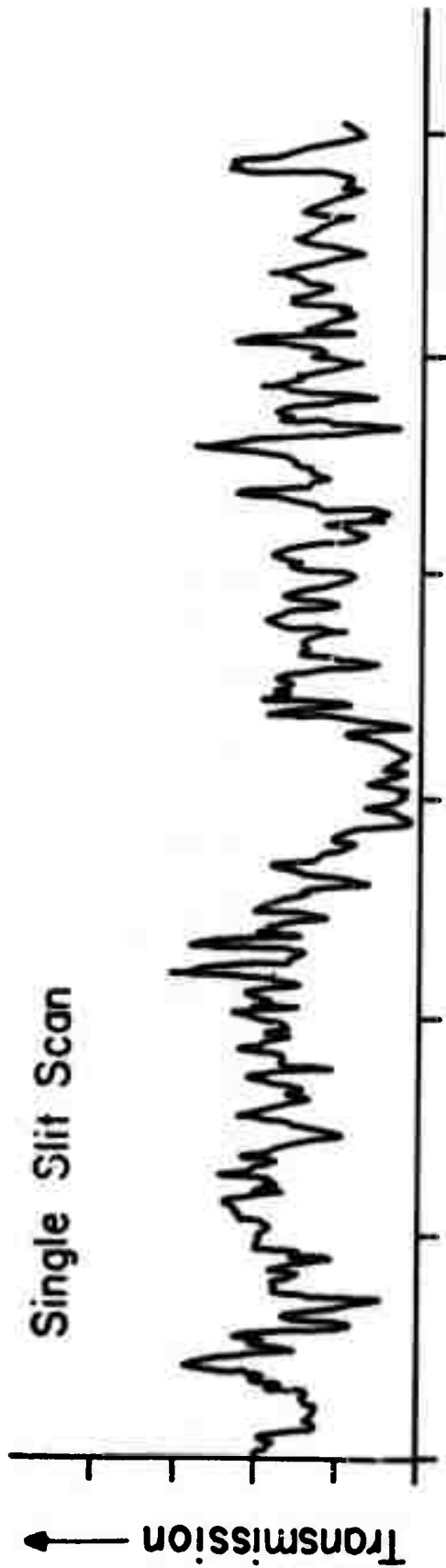


Fig. 4. Water Vapor Absorption At Three Pressures Over 92 Meter Path Length.



High Resolution Spectra. (a) Water Vapor At  $P = 0.300$  mm, 92 m Path Length. (b) Carbon Dioxide At  $P = 20$  mm, 2.2 m Path Length.

Fig. 7 High resolution spectra. (a) Water vapor at  $P = 0.300$  mm, 92m path length. (b) carbon dioxide at  $P = 20$ mm, 2.2m path length.



References

1. J. Strong, Appl. Opt. 10, No. 6, 1439 (June, 1971).
2. J. A. Decker, Jr., Appl. Opt. 10, No. 3, 510 (March, 1971).
3. J. Strong, U.S. Patent No. 2,743,646.
4. E. D. Nelson and M. L. Fredman, J. Opt. Soc. Am. 60, No. 12, 1664 (December, 1970).
5. F. W. Dalby and H. H. Nielsen, J. Chem. Phys. 25, No. 5, 934 (November, 1956).
6. International Union of Pure and Applied Chemistry, Commission on Molecular Structure and Spectroscopy, Tables of Wavenumbers for the Calibration of Infra-red Spectrometers (Washington: Butterworths, 1961), pp. 654-55.